UNIVERSIDAD DE INVESTIGACIÓN DE TECNOLOGÍA EXPERIMENTAL YACHAY

Escuela de Ciencias Físicas y Nanotecnología

TÍTULO: Radioactivity Influence by ^{40}K in the KM3NeT DOMs

Trabajo de integración curricular presentado como requisito para la obtención del título de Físico

Autor:

Alcívar Espín Juan David

Tutor:

Ph.D. - Yepes Ramírez Harold

Urcuquí, Diciembre 2020

SECRETARÍA GENERAL
(Vicerrectorado Académico/Cancillería)
ESCUELA DE CIENCIAS FÍSICAS Y NANOTECNOLOGÍA
CARRERA DE FÍSICA
ACTA DE DEFENSA No. UITEY-PHY-2020-00025-AD

A los 7 días del mes de diciembre de 2020, a las 16:00 horas, de manera virtual mediante videoconferencia, y ante el Tribunal Calificador, integrado por los docentes:

Presidente Tribunal de Defensa	Dr. PINTO ESPARZA, HENRY PAUL , Ph.D.
Miembro No Tutor	Dr. BRAMER ESCAMILLA , WERNER , Ph.D.
Tutor	Dr. YEPES RAMIREZ, HAROLD , Ph.D.

El(la) señor(ita) estudiante **ALCIVAR ESPIN, JUAN DAVID**, con cédula de identidad No. **1725605149**, de la **ESCUELA DE CIENCIAS FÍSICAS Y NANOTECNOLOGÍA**, de la Carrera de **FÍSICA**, aprobada por el Consejo de Educación Superior (CES), mediante Resolución **RPC-SO-39-No.456-2014**, realiza a través de videoconferencia, la sustentación de su trabajo de titulación denominado: **RADIOACTIVITY INFLUENCE BY 40K IN THE KM3NET DOMS**, previa a la obtención del título de **FÍSICO/A**.

El citado trabajo de titulación, fue debidamente aprobado por el(los) docente(s):

Tutor	Dr. YEPES RAMIREZ, HAROLD , Ph.D.

Y recibió las observaciones de los otros miembros del Tribunal Calificador, las mismas que han sido incorporadas por el(la) estudiante.

Previamente cumplidos los requisitos legales y reglamentarios, el trabajo de titulación fue sustentado por el(la) estudiante y examinado por los miembros del Tribunal Calificador. Escuchada la sustentación del trabajo de titulación a través de videoconferencia, que integró la exposición de el(la) estudiante sobre el contenido de la misma y las preguntas formuladas por los miembros del Tribunal, se califica la sustentación del trabajo de titulación con las siguientes calificaciones:

Tipo	Docente	Calificación
Presidente Tribunal De Defensa	Dr. PINTO ESPARZA, HENRY PAUL , Ph.D.	9,5
Miembro Tribunal De Defensa	Dr. BRAMER ESCAMILLA , WERNER , Ph.D.	10,0
Tutor	Dr. YEPES RAMIREZ, HAROLD , Ph.D.	9,0

Lo que da un promedio de: **9.5 (Nueve punto Cinco)**, sobre 10 (diez), equivalente a: **APROBADO**

Para constancia de lo actuado, firman los miembros del Tribunal Calificador, el/la estudiante y el/la secretario ad-hoc.

Certifico que *en cumplimiento del Decreto Ejecutivo 1017 de 16 de marzo de 2020, la defensa de trabajo de titulación (o examen de grado modalidad teórico práctica) se realizó vía virtual, por lo que las firmas de los miembros del Tribunal de Defensa de Grado, constan en forma digital.*

ALCIVAR ESPIN, JUAN DAVID
Estudiante

Dr. PINTO ESPARZA, HENRY PAUL , Ph.D.
Presidente Tribunal de Defensa

HENRY PAUL PINTO ESPARZA
Digitally signed by HENRY PAUL PINTO ESPARZA
Date: 2020.12.13 22:42:23 -05'00'

Dr. YEPES RAMIREZ, HAROLD , Ph.D.
Tutor

CERTIFICACIÓN ELECTRÓNICA
BANCO CENTRAL DEL ECUADOR
Firmado Digitalmente por: HAROLD YEPES RAMIREZ
Hora oficial Ecuador: 08/12/2020 13:44

Dr. BRAMER ESCAMILLA , WERNER , Ph.D.
Miembro No Tutor

YASELGA NARANJO, CARLA
Secretario Ad-hoc
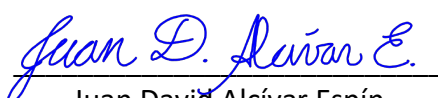
AUTORÍA

Yo, **JUAN DAVID ALCÍVAR ESPÍN**, con cédula de identidad 1725605149, declaro que las ideas, juicios, valoraciones, interpretaciones, consultas bibliográficas, definiciones y conceptualizaciones expuestas en el presente trabajo; así cómo, los procedimientos y herramientas utilizadas en la investigación, son de absoluta responsabilidad de el/la autora (a) del trabajo de integración curricular. Así mismo, me acojo a los reglamentos internos de la Universidad de Investigación de Tecnología Experimental Yachay.

Urcuquí, diciembre 2020.

Juan David Alcívar Espín
CI: 1725605149

AUTORIZACIÓN DE PUBLICACIÓN

Yo, **JUAN DAVID ALCÍVAR ESPÍN,** con cédula de identidad 1725605149, cedo a la Universidad de Tecnología Experimental Yachay, los derechos de publicación de la presente obra, sin que deba haber un reconocimiento económico por este concepto. Declaro además que el texto del presente trabajo de titulación no podrá ser cedido a ninguna empresa editorial para su publicación u otros fines, sin contar previamente con la autorización escrita de la Universidad.

Asimismo, autorizo a la Universidad que realice la digitalización y publicación de este trabajo de integración curricular en el repositorio virtual, de conformidad a lo dispuesto en el Art. 144 de la Ley Orgánica de Educación Superior.

Urcuquí, diciembre de 2020.

Juan David Alcívar Espín
CI: 1725605149

Dedicatoria

A mis padres y hermanos por su apoyo incondicional y fortaleza para cumplir mis metas.

Juan David Alcívar Espín

Acknowledgements

Resumen

KM3NeT es una colaboración internacional que se encuentra construyendo y operando la infraestructura de investigación submarina más grande, multidisciplinaria y multipropósito del hemisferio norte que albergará la siguiente generación de telescopios de neutrinos. Estos están siendo ubicados en dos sitios del Mar Mediterráneo que corresponden a ORCA y ARCA, entre 2500-3500 metros de profundidad. El objetivo de ORCA es estudiar la jerarquía de masas de neutrinos y los parámetros de oscilación con neutrinos atmosféricos, mientras que ARCA está optimizado para detectar y estudiar fuentes de alta energía de neutrinos cósmicos. Para cumplir su propósito KM3NeT está compuesto de cientos de tubos fotomultiplicadores (PMTs) que detectan luz Cherenkov inducida por leptones cargados que superan la velocidad de la luz en el medio, producidos por la interacción de neutrinos. Treinta y un PMTs, de 3-pulgadas cada uno, se encuentran dentro de un módulo óptico digital (DOM) protegido por una esfera de 17-pulgadas en diámetro. Este contenedor está hecho de un vidrio borosilicato (Vitrovex) de 14-mm de grosor, resistente a las altas presiones del fondo del mar. Se presume que el Vitrovex contiene rastros de isotopos como ^{40}K, ^{232}Th, y ^{238}U, de los cuales sus subproductos se liberan en el agua marina y dentro del Vitrovex. ^{40}K libera la cantidad más significativa de electrones relativistas que exceden el umbral de energía Cherenkov, causando señales que constituyen un fondo óptico que debe ser separado de las señales inducidas por la interacción de neutrinos con el medio.

Este estudio experimental busca tasas de coincidencia producidos en los DOMs de KM3NeT, que se sospecha son causadas por el decaimiento radioactivo de ^{40}K, ^{232}Th, ^{238}U y discute su influencia como fondo óptico para KM3NeT. La caracterización de este fondo óptico, previo a la ubicación de líneas de DOMs es fundamental para entender mejor el comportamiento de telescopios de neutrinos en el fondo del mar.

Palabras Clave:

KM3NeT, radioactividad, fondo, DOM, DOM, Vitrovex, ^{40}K.

Abstract

The KM3NeT Collaboration is building and operating the biggest deep-sea multidisciplinary and multipurpose research infrastructure of the Northern Hemisphere that will host the next generation neutrino telescopes. They are being located at two sites in the Mediterranean Sea, at a depth of about 2500-3500 meters, at ORCA and ARCA sites. The goal of ARCA is to detect and study high-energy cosmic neutrino sources; meanwhile, ORCA aims to study neutrino mass hierarchy and oscillation parameters from atmospheric neutrinos. For this purpose, KM3NeT is suited with arrays of thousands of Photo-Multiplier Tubes (PMTs) for detecting the Cherenkov light induced by charged leptons, produced by neutrino interactions, exceeding the phase velocity of light in the medium or surroundings. Thirty-one, 3-inch PMTs are contained inside Digital Optical Modules (DOMs), which are protected by a 17-inch spherical case. This vessel is made of 14-mm thick borosilicate glass (Vitrovex), resistant to the high pressure of the harsh deep-sea environment. Vitrovex seems to contain traces of isotopes such as ^{40}K, ^{232}Th, and ^{238}U, which its sub-products are released in seawater and inside Vitrovex itself. ^{40}K releases the most significant amount of relativistic electrons that exceed Cherenkov threshold energy in the medium, causing signals that constitute an Optical Background that must be disentangled from signals induced by neutrino interactions with the environment.

This experimental study looks for coincidence rates in KM3NeT DOMs suspected to be caused by the radioactive decay of ^{40}K, ^{232}Th, ^{238}U and discusses their influence as optical background for KM3NeT. Characterization of the optical background, prior to the deployment of Detection Units DUs, is fundamental to better understand the behavior of the telescope in the deep sea.

Key Words:
KM3NeT, radioactivity, background, DOM, Vitrovex, ^{40}K.

Contents

List of Figures

List of Tables

Chapter 1

Problem Statement

KM3NeT is an international collaboration building the next generation neutrino telescopes in the bottom of the Mediterranean Sea, ARCA and ORCA. These telescopes aim to look and study high energy neutrinos (E_ν>10 TeV) coming from distant astrophysical sources and to study Neutrino Mass Hierarchy (NMH) and oscillation parameters (MeV < E_ν< GeV) with atmospheric neutrinos, respectively. KM3NeT is affected by backgrounds coming from sources external or even proper to the detector; these can be either physical or optical. The physical background is induced by muons or neutrinos produced in cosmic-ray interactions in Earth's atmosphere. Atmospheric muons can penetrate the water above the detector and give rise to a reducible background. On the other hand, atmospheric neutrinos, coming from underneath Earth, make part of an irreducible background. The optical background, which is the focus of study in this project, is induced by random light, not associated with particles traversing the detector. This background is produced either by the many bioluminescent life forms that inhabit the depths of the sea or by the decay of naturally occurring radioactive materials such as ^{40}K .

For detectors sensitive to signals produced by background sources, the concept of radiopurity of constituent materials is vital for the reliability of collected data. To avoid background induced by radioactive sources, as much as possible, materials used for the construction of the detector and the place of deployment must be carefully selected. After all controls, some traces of radioactive materials may still appear inside the detector and cause a background. This study identifies the possible sources and discusses the uncertainty that small traces of radioactive materials might cause in the estimation of the optical background. In particle physics experiments, the background coming from materials used in the construction of detectors may be used as a calibration tool, and reducible by coincidence methods to an acceptable level.

As mentioned previously, an optical background source that affects KM3NeT detectors is the one produced by traces of possible radioactive materials left from the integration of constituent materials. When these elements decay mostly through β emission, electrons or positrons with sufficient energy and velocity are released to produce Cherenkov light and a steady, isotropic background. This constant background generates a signature that has to be identified

and isolated from the neutrino signal induced by the interactions of charged leptons. ^{40}K is known to be contained in the mineral salts of seawater and apparently in the DOMs glass vessel (Vitrovex), in agreement to the manufacturer technical specifications. Some studies performed to Vitrovex show tiny amounts of several radioactive elements, having ^{40}K the highest mass-specific activity (Bq/kg). It is essential to characterize the effect produced by traces of ^{40}K in the lab with a controlled environment, prior to the deployment of the detectors in the sea, to prevent the influence of additional optical background components.

KM3NeT has simulated the signature produced by ^{40}K and other radioisotopes like ^{232}Th and ^{238}U contained in Vitrovex, once the DOMs are in the deep sea. In this experimental work, the signature produced by traces of radioactive elements is studied in the laboratory with data from a dedicated experimental test bench and fitting the conditions of the simulation as much as possible to the experiment.

1.1   General and Specific Objectives

General Objective

The general objective of this work is to study, in the lab, the signature produced by traces of elements such as ^{40}K contained in Vitrovex prior to the deployment of DUs in the deep-sea, and to discuss the importance of the radiopurity of materials used in the construction of KM3NeT.

Specific Objectives

In order to achieve the general objective, the following specific objectives are pursued:

- Study Vitrovex, the material that frames DOMs, a basic detection element of KM3NeT.

- Study the optical background induced by the decay of ^{40}K in Vitrovex, and the possible contribution of ^{232}Th and ^{238}U, and how they produce Cherenkov signals.

- Use of available KM3NeT customized software tools to analyze data obtained in the experimental test bench designed for this work.

- Compare the experimental data with simulations that best fit the obtained results, and estimate the contribution of ^{40}K in Vitrovex.

Beyond the importance of radioactivity in the selection of radiopure materials for high energy physics experiments, other peaceful uses in society are present in agriculture, plague control, fertilisers, diagnosis, medicine, therapy, and industry among others. All these uses are aimed to improve the daily life of communities.

Chapter 2

Scientific Context

2.1 Science Behind the Experiment

Until a few decades ago, most of the information of our Universe was collected from photons in the visible spectrum[2]. The detection was possible since photons have some features that allow them to dodge electromagnetic and physical barriers. Even though photons have such distinctive features, it is challenging to detect the information they carry from distant, deep, and dense places of the Universe[2]. In order to enhance the knowledge, the study of alternative cosmic messengers became relevant, since each originates at different astrophysical process. Multi-messenger astronomy allows to obtain complementary information from high energy particles like Cosmic Rays (CRs), Electromagnetic Radiation (EM) , ripples in space-time in the form of Gravitational Waves (GW), and neutrinos (ν).

Neutrinos are elementary particles that are part of the lepton family of the Standard Model (SM) of particle physics, as can be observed in Figure 2.1. Nowadays it is known that neutrinos have tiny masses, and are changeless leptons, they do not experience strong interactions but only interact through the weak force. The name neutrino means "little neutral one", and refers to the fact that they carry no electrical charge. The fact that neutrinos have nearly no mass make them zip throughout the cosmos at speeds close to the speed of light. Due to these features, neutrinos' cross-section is significantly reduced and requires large detectors and exposure time. In the SM, neutrinos come in three flavors, linked to the three charged leptons: electron, muon, and tau. Neutrinos provide evidence that new physics beyond the SM exist, as this model does not predict the non-zero mass and the mixing among neutrino families, opening the Beyond Standard Model (BSM) physics.

Neutrinos are interesting subatomic particles created in a wide variety of processes: in particle accelerators and in nuclear reactors, in the core of stars, during the explosive collapse of supernovas and when radioactive elements decay. They were first postulated as an answer to a scientific enigma. In the 19th century, researchers were puzzling over a phenomenon known as beta (β) decay, where the nucleus inside an atom spontaneously emits an electron (β^- decay) or a positron (β^+ decay). β decay seemed to violate two fundamental physical laws: conservation of energy and conservation of momentum. In β decay, the final configuration of particles seemed to have slightly too small energy, and the proton was standing still rather than being knocked in the opposite direction of the electron/positrons.

3
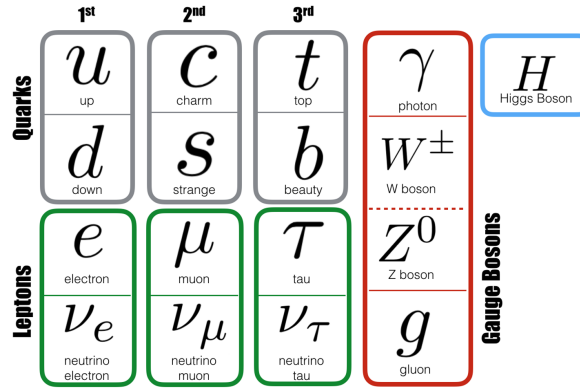
Figure 2.1: Model of particle physics where three flavour of neutrinos are represented. Adapted from Reference[3].

In 1930, Wolfgang Pauli introduced neutrinos and antineutrinos as an explanation to the continuous energy spectrum of the electrons emitted by β decays[4]. Neutrinos follow nuclear reactions such as β decay[5] where,

$$
\begin{aligned}
n &\rightarrow p + e^- + \bar{\nu}_e \qquad (\beta^- decay), \\
p &\rightarrow n + e^+ + \nu_e \qquad (\beta^+ decay),
\end{aligned}
\tag{2.1}
$$

or the reaction generated by hadronic processes, as protons with nuclei in the atmosphere, which produces muons and neutrinos[4]:

$$
\begin{aligned}
p + N &\rightarrow \pi^{\pm/0} + X, \\
\pi^\pm &\rightarrow \mu^\pm + \nu_\mu/\bar{\nu}_\mu.
\end{aligned}
\tag{2.2}
$$

Muon and antimuon decay subsequently into an electron plus a muon- neutrino, and positron plus a muon-antineutrino respectively:

$$
\begin{aligned}
\mu^- &\rightarrow e^- + \bar{\nu}_e + \nu_\mu, \\
\mu^+ &\rightarrow e^+ + \nu_e + \bar{\nu}_\mu.
\end{aligned}
\tag{2.3}
$$

Since their discovery, neutrinos have continually defied scientists' expectations. The Sun produces colossal numbers of neutrinos that bombard the Earth, and in the mid 20th century, researchers built detectors to search for these neutrinos. However, their experiments kept showing a discrepancy, detecting only about one-third of the neutrinos that had been predicted. Eventually, physicists realized that neutrinos are the uncharged partners of the charged leptons, electrons, muons and tau, and named them after those. As neutrinos pass through the distance between The Sun and our planet, they oscillate between flavors, which is why those early experiments which had only been designed to search for one flavor kept missing two-thirds of their total number.

Neutrino interactions

Although neutrinos are everywhere, they remain a mystery to physicist since they are so hard to detect. There are two ways that neutrinos interact with matter: Charged Current (CC) interaction where the neutrino is changed to a charged lepton of the same family, and Neutral Current (NC) interaction where neutrino keeps unchanged. The CC interaction, as shown in Equation 2.4, is one of the ways in which subatomic particles can interact by the weak force. Bosons W^+ and W^- mediates the interaction with an electrically charged particle. During the process, W bosons induce the emission of an electron/positron, absorption, or change the flavor of quark as well as electrical charge. CC interaction is the most easily detected of the interactions of the weak force.

$$\nu_\ell + N \rightarrow \ell + X \tag{2.4}$$

The NC interaction is another way in which subatomic particles can interact through the weak force. The Z-boson mediates this type of interaction, and it is electrically neutral. The exchange of a Z-boson leaves the interacting particles' quantum numbers unaffected, except for a transfer of momentum, spin, and energy. By contrast to W, exchanges of Z-boson involve no transfer of electrical charge, so it is referred to as a "neutral current". The word "current" merely refers to the Z-bosons' movement between other particles. Two types of NC interactions are differentiable: the elastic scattering where the starting and final hadronic states are different, and the inelastic scattering where the starting and final products are the same.[6][7]

$$\begin{aligned}
\nu_\ell + e^- &\rightarrow \nu_\ell + e^- &&\textit{(Elastic)} \\
\nu_\ell + N &\rightarrow \nu_\ell + X &&\textit{(Inelastic)}
\end{aligned} \tag{2.5}$$

Neutrino Oscillations and Mass Hierarchy

Experiments have established that neutrinos produced in defined flavor state, for example muon-neutrino ν_μ, have a non-zero probability of being detected in a different flavor state, for example, electron-neutrino ν_ℓ. The discovery that neutrinos have mass, and that they change flavor as a consequence of neutrino oscillation explain the reduction in solar electron neutrinos and the missing neutrino flux mentioned previously. The probability in changing flavor depends on the energy of the neutrino, and the distance traveled between the source and the detector[8]. The prove that neutrinos have mass implies that a neutrino produced as a superposition of mass eigenstates (ν_1, ν_2, ν_3), such as a neutrino ν_α with a well defined flavor has certain probability of being measured as a different flavor neutrino ν_β, being $\alpha, \beta = e, \mu, \tau$. This probability $P_{\alpha\beta}$ depends on the energy of the neutrino E, the distance of propagation between the source and the detector L, the mass-squared difference $\Delta m_{ij}^2 \equiv m_i^2 - m_j^2$, and it is described by the PMNS matrix (Pontecorvo–Maki–Nakagawa–Sakata) U, shown in Equation 2.6, which is product of three rotation matrices related to the mixing angles (θ_{12}, θ_{13}, and θ_{23}) and to the complex CP leptonic phase (δ), where $c_{ij} \equiv \cos\theta_{ij}$ and $s_{ij} \equiv \sin\theta_{ij}$[8][9]:

$$U = \begin{pmatrix} 1 & 0 & 0 \\ 0 & c_{23} & s_{23} \\ 0 & -s_{23} & c_{23} \end{pmatrix} \begin{pmatrix} c_{13} & 0 & e^{-i\delta}s_{13} \\ 0 & 1 & 0 \\ e^{-i\delta}s_{13} & 0 & c_{13} \end{pmatrix} \begin{pmatrix} c_{12} & s_{12} & 0 \\ s_{12} & c_{12} & 0 \\ 0 & 0 & 1 \end{pmatrix} \tag{2.6}$$

In a three-neutrino scheme, two independent mass-squared differences exist. One of these differences relate the atmospheric neutrino sector ($\Delta m^2_{atm} \approx 2.52 \times 10^{-3} \text{eV}^2$), meanwhile the other is responsible for the oscillations observed in solar and long baseline reactor experiments ($\Delta m^2_{sol} \approx 7.42 \times 10^{-5} \text{eV}^2$)[10]. Currently, the biggest challenge in this sense is focused on precision measurements for neutrino oscillation parameters.
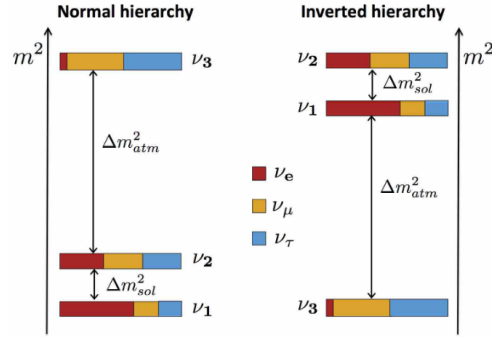
Figure 2.2: Scheme of the two distinct neutrino mass hierarchies (normal and inverted). The color code indicates he fraction of each neutrino flavor (e, μ, τ) present in each of the mass eigenstates (ν_1, ν_2, ν_3). Adapted from Reference[9].

Despite the discoveries, the order of neutrino mass eigenstates has no been found which makes the determination of the NMH a major unknown in neutrino science. By fixing $\Delta m^2_{21} = \Delta m^2_{sol} > 0$, two solutions remain still possible depending on the sign of Δm^2_{31}: Normal Hierarchy (NH) where $m_1 < m_2 < m_3$ and Inverted Hierarchy (IH) where $m_2 < m_3 < m_1$. Both possible solutions are shown in Figure 2.2. The determination of the NMH is fundamental. From a theoretical point of view, it is important to constrain the models that aim to explain the origin of mass in the leptonic sector and the differences in the mass spectrum of leptons and quarks. From an experimental point of view, NMH is important since it can have a strong impact on the potential performance of the next generation of experiments to determine unknown parameters like the absolute value of the neutrino masses[9].

Terrestrial Neutrino Sources

Neutrinos have different origins including neutrinos generated at the Earth. Neutrinos can be produced from human activity at particle accelerators and nuclear reactors. The first one produces high energy neutrinos that can reach up to hundreds of GeV, and are used to study the structure of nucleons, and the weak interaction. The second ones are abundant, produced by nuclear reactions inside reactor cores. These neutrinos have low energy at around of a few MeV. Neutrinos could also be produced inside the planet from natural occurring radioactivity, despite the quantity, these neutrinos get easily confused with the ones produced in nuclear plants[11]. Finally, when particles coming from somewhere in space penetrate to the Earth's atmosphere, like cosmic rays, it interacts with atomic nuclei that generate particle showers. In this process, atmospheric neutrinos are created[11].

Extra-Terrestrial Neutrino Sources

Other sources of neutrinos are the ones coming from outside the Earth. These could have a galactic origin and some others extra-galactic origin as listed below.

Sources producing neutrinos in the galaxy:

- **The Sun** is a well established source of neutrinos, as they are created from thermonuclear fusion inside the star. Neutrinos produced at this source are relatively weak as its energy reaches a few MeV. They are produced from different nuclear reactions but most of neutrinos are generated from proton-proton chain interaction $(p + p \rightarrow {}^2\text{H} + e^- + \nu_e)$[11].

- **Pulsar Wind Nebula (PWNe)** refers to particles accelerated to relativistic energy that can interact with the surrounding matter. The production of neutrinos is possible since it has been suggested the existence of a hadronic part in the pulsar wind, charged pions (π^+, π^-) decay. Gamma-rays are produced by the decay of neutral pions (π^0), however, most of the gamma process is commonly assumed to be leptonic.

- **Supernova Remnants (SNRs)** are remnants of a supernova that presumably are a source of cosmic rays, and so a possible source of neutrinos. The initial explosion forms a shock wave that travels through the galactic medium. The gamma-ray spectra measured from SNRs can be used to estimate its neutrino rate.

- **Microquasars** are binary systems that are composed of star accompanied by a neutron star or a black hole. The compact object aggregates mass from the other star and makes relativistic jets perpendicular to the disc of accretion. In has been argued that these objects might emit high energy neutrino fluxes much bigger than predicted from their gamma-ray spectra.

Some sources producing neutrinos outside the galaxy are described below:

- **Active Galactic Nuclei (AGN)** refers to galaxies composed of a massive black hole surrounded by an accretion disc. They are particular for having a relativistic jet coming out of the center of the disc from where high energy gamma rays and neutrinos are expected along with the jet emission.

- **Starburst Galaxies** present an elevated rate of star formation and have been suggested as neutrino sources since synchrotron radiation at radio wavelengths coming from the dense core region implies the existence of relativistic electrons. Neutrinos can result from proton-proton interactions assuming that protons are also accelerated along with electrons.

- **Gamma-Ray Bursts (GRBs)** are phenomena emitting gamma-ray fluxes that surpass all other gamma-ray sources since they eject matter in ultra-relativistic jets. GRBs are randomly distributed in the sky plane, which contributes to the assumption that they correspond to extra-galactic objects. They are usually associated with the merge of binary systems composed of two neutron stars, or a neutron star and a black hole, and additionally, they are associated with the collapse of massive stars that form black holes.[12][13]

2.2 Radioactivity and Cherenkov Radiation

Radioactivity

Radioactivity is the emission of energy (radiation) coming from a nuclear reaction or as the result of the spontaneous decay of unstable atomic nuclei. Radioactive decay refers to the process where unstable atomic nuclei decay by losing energy and releasing energetic particles (α-particles, β- particles, γ-ray photons) directly from the nucleus or the electron shells. The rate of decay or activity of a radionuclide is proportional to its mass, and it is measured in becquerels (Bq), as one Bq is equivalent to one disintegration per second. The velocity of decay is therefore the rate at which the number of radioactive nuclei vary in a unit of time. The radiation resulting from the decay of radionuclide might occur in various types, energies, intensities and more than one mode of decay[14].

- α-decay is the radioactive process in which an atomic nucleus emits an α-particle and becomes a nucleus with a mass number and atomic number four units smaller. An α-particle is considered to be Helium-4 ($^4H^{2+}$). This type of decay is particular of heavy nuclei atoms: $^A_ZX \rightarrow ^{A-4}_{Z-2}Y + ^4_2H^{2+} = ^{A-4}_{Z-2}Y + \alpha$.

- β-decay is the radioactive process where an energetic and fast electron or positron (β-particle) is emitted as shown in Equation 2.1. Two channels of decay exist, β^- and β^+, produced by the emission of e^- and e^+ respectively. In one hand, for unstable nuclei with excess of neutrons, β^- decay is possible. In this case, a neutron becomes a proton, and an electron and an antineutrino electron are released. In the other hand, for nuclei with excess of protons, β^+ decay is possible. In this case, a proton becomes a neutron by releasing a positron and a neutrino electron.

- γ-radiation is a type of electromagnetic radiation. It is usually produced by radioactive elements, by the process of positron-electron annihilation, or by change of energy levels at the subatomic scale. γ-radiation is highly energetic making it able to penetrate the matter more deeply that α and β radiation.

Radioactivity in seawater

Radioactivity in seawater is influenced by natural occurring processes and by wastes produced in continental masses that ended up being poured into the oceans. At first, it was associated with certain minerals but soon was discovered that basically all minerals and natural waters display this property at some degree. The natural radioactivity of water appears mainly from its mineral composition. Among the natural nuclei that appear in water are potassium, uranium and thorium decay series. The radioactivity in the oceans surface averages 13.6 Bq/kg worldwide and most of the activity come from a single natural radio-nuclei: ^{40}K. The content of traces of uranium ranges 1.1 to 1.7×10^{-8} g/l of water and thorium ranges around 0.5×10^{-6} g/l of seawater[15][16]. The Mediterranean Sea (KM3NeT site) is not exempt from containing particles of radioactive materials since some traces have been measured in the coastal sediments of the western Mediterranean Sea. The recorded activity levels are within the range measured worldwide. Beside the natural occurring minerals, radioactivity is in turn influenced by the the amount of settlements and types of industrial labors around the area. The activity in the Eastern Mediterranean waters has been measured and averages 14.6 Bq/kg, which is above the average[17][16]. Deep-sea detectors must have well identified the radioactive sources

(a)   (b)
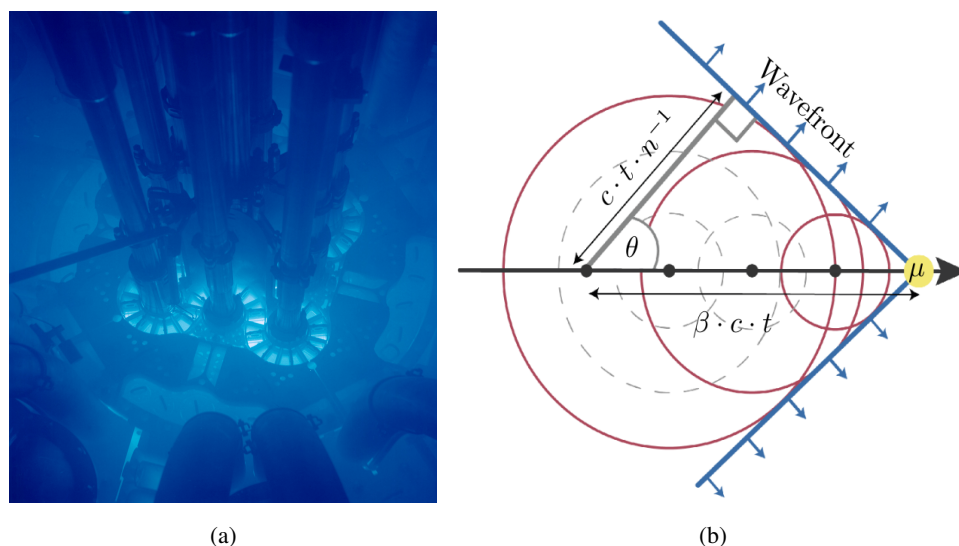
Figure 2.3: Cherenkov Radiation. (a) Light produced by Cherenkov effect in a nuclear reactor. (b) Scheme showing the Cherenkov cone produced by a muon (μ). Adapted from Reference[18].

and contamination in the detection medium as these factors make part of the background. KM3NeT has identified an average rate contribution of 6-8 kHz per 3-inch PMT due to radioactive decay in seawater, including the dark count rate[9].

Cherenkov Radiation

When a travelling particle crosses a transparent medium moving with a velocity faster than the group velocity of light in that medium, it will cause emission of electromagnetic radiation (photons) all along its trajectory. This phenomenon is known as Cherenkov radiation or Cherenkov effect and it is produced as response, when the electric field of the particle polarises the medium. As electrons undergo de-excitation, radiation is emitted. A schematic of this process is shown on Figure 2.5b[18]. A typical example of this effect is the blue glow associated with the sub-products released from fuel rods submerged in water in nuclear reactors, as it can be observed on Figure 2.3a. Cherenkov effect is the most common method for the indirect detection of neutrinos in large volume detectors such as KM3NeT. Other techniques to detect neutrinos also exist and are applied depending on energy range and issue of study such as radio detectors, radio-chemical methods and tracking calorimeters. The configuration of the KM3NeT DOMs allow for the recognition of multiple Cherenkov photons from decay of radioactive elements, the bioluminescent activity in the surrounding environment, and the light emitted by secondary charged particles produced in neutrino interactions with seawater or with rocks beneath the sea[18][19][5]. The emission of Cherenkov light occurs in the form of a cone with an opening angle θ relative to the travel direction of the particle. Following

Figure 2.5b, the angle is given by:

$$\cos(\theta) = \frac{1}{n} \cdot \frac{ct}{\beta ct} = \frac{1}{n\beta},$$ (2.7)

where n is the refractive index of the medium, and $\beta = v/c$ is the fraction of the velocity at which the particle is moving relative to the speed of light in vacuum. The emission of Cherenkov light occurs in a rotationally symmetric way, where a cone of expanding light appears along and around the path of propagation of the particle[19]. The number of emitted photons is represented by x and the wavelength is given by Frank-Tamm formula[20],

$$\frac{d^2N}{dxd\lambda} = \frac{2\pi\alpha z^2}{\lambda^2} \cdot \sin^2(\theta).$$ (2.8)

In a relativistic track, $\beta = 1$, in water where $n = 1.33$, around 250 cm^{-1} optical photons are produced in a range of 300 to 500 nm, which is the usual detection range of optical sensors used in neutrino telescopes. The angle formed for a relativistic track is $\theta = \arccos(1/n) \approx 41°$. When particles' speed is below c/n, the result of the cosine function would be greater than 1, and therefore no valid angle can be calculated, meanwhile at speeds above the Cherenkov threshold an emission direction, and therefore the opening angle of the Cherenkov cone can be calculated. The Cherenkov threshold energy is given by,[20]

$$E \geq m \cdot \left(\frac{1}{\sqrt{1 - \frac{1}{n^2}}} - 1 \right).$$ (2.9)

It is worthy to mention that in water the Cherenkov threshold, or the minimal energy that a particle must have to produce Cherenkov radiation is $E_e \approx 0.25\text{MeV}$ for electrons, and $E_\mu \approx 55\text{MeV}$ for muons[19][20].

2.3 Experimental Infrastructure: KM3NeT, DOMs and Vitrovex

KM3NeT aims to build an infrastructure that will be composed of three building blocks. A building block is a 3D array of DOMs housing PMTs disposed to detect Cherenkov light generated by relativistic particles passing through the detection medium. Each building block will be composed of 115 DUs[9], as shown in Figure 2.4a. The concept behind the construction and operation of building blocks is modular, which allows for a phased and distributed implementation. Two of the three building blocks will be dedicated to ARCA (Astroparticle Research with Cosmics in the Abyss), which will have a sparse configuration with comparable volume and improved resolution. The other building block will be dedicated to ORCA (Oscillation Research with Cosmics in the Abyss), which will have a denser configuration. Some features that make ARCA and ORCA ideal instruments to study neutrinos and the cosmos are the transparency of the deep waters, the size of the detector, and its geographical location. A comparison of sizes between ARCA and ORCA can be observed in Figure 2.4b[9].

ARCA is under construction at the facility of KM3NeT-It, 100 km from the coast of Portopalo di Capo Passero in Sicily, Italy.[9] Every DU of ARCA is a vertical line with a height of 700 m anchored at around 3500 m of depth. ARCA

(a)   (b)
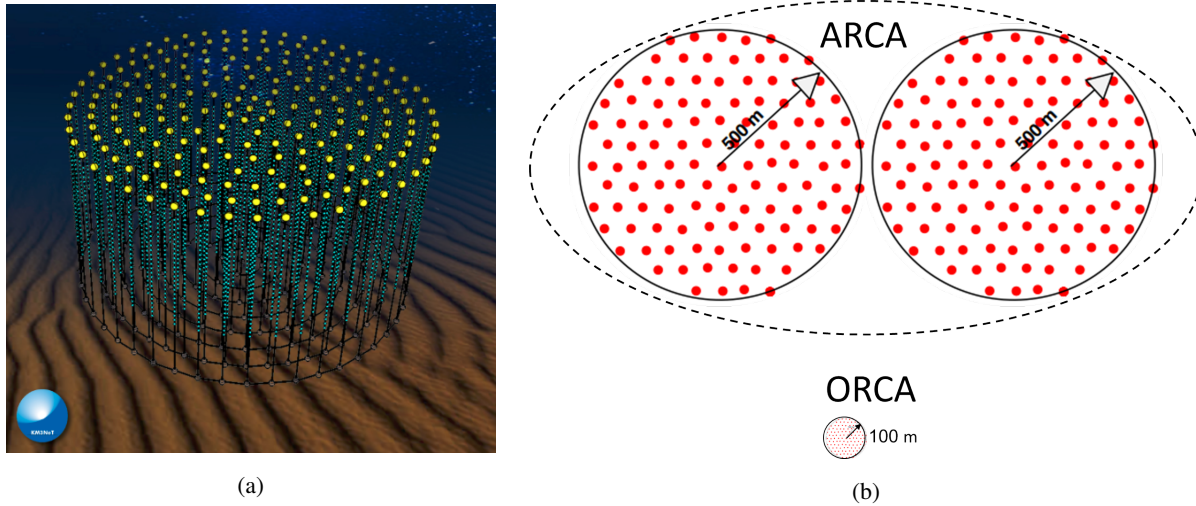
Figure 2.4: KM3NeT layouts (a) KM3NeT Building Block composed of vertical DUs, holding DOMs.[9] (b) Relative size of ARCA and ORCA. It can be observed the difference between the effective area of both detectors. Adapted from Reference[9].

is being built to detect neutrinos with energies in a range of several GeV to PeV[21]. Its location in the Mediterranean Sea provides a strategic position to map about 87% of the sky including most of the Galaxy and Galactic Center, where other astronomical detectors have observed particular phenomena.[9] ORCA is being deployed at the facility of KM3NeT-Fr, 40 km from the coast of Toulon, France. DOMs will be arranged on vertical DUs with a height of around 200 m and anchored at about 2500 m of depth. It has a denser configuration than ARCA, and its design allows to detect neutrinos with energy ranges as low as GeV.[9]

A DU is a collection of 18 DOMs arranged along a vertical structure, communicated by an electro-optical cable. DOMs are held together by two 4 mm ropes made of Dyneema®, the strongest and lightest fiber available in the market. Each DOM is secured by the titanium collar that surrounds it. For ARCA, DOMs have an spacing of 36 m, and 100 m between DUs. In the case of ORCA, DOMs have an spacing of 9 m, and 40 m between DUs. In the bottom part, DUs are anchored to the seabed by a dead-weight that maintains them firmly connected. In the top extreme, a buoy is connected to minimize the horizontal displacement, relative to the base, caused by the drag force of sea currents. Attached to the Dyneema ropes runs an electro-optical cable and an oil-filled pressure-balanced tube that contains a pair of copper wires that transmit 400 VDC of voltage and the data for the 18 DOMs that compose the DU. Additionally, a breakout box converts the 400V to useful 12V[9].

As mentioned earlier, KM3NeT is composed of DOMs distributed along large volumes of transparent water in the depths of the Mediterranean Sea. DOMs register the arrival time of the Cherenkov light throughout the detection volume, the geometrical position of the sensors and the amount of light received. Data collected by DOMs travel to powerful computers in shore-stations through an optical fiber network. Gathered data is centralized in the "Centre de Calcul de l'IN2P3/CNRS – USR6402", then available for the KM3NeT collaboration for detailed technical and

| (a) | (b) |
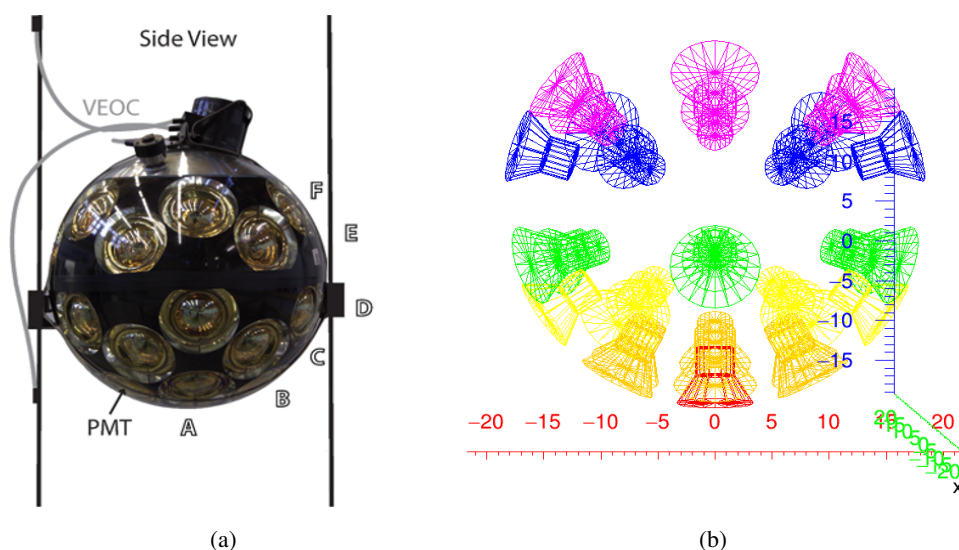
Figure 2.5: The KM3NeT DOM. (a) DOM marked with the names of each row of PMTs. (b) 3D reference of the PMTs into the DOM, each row of PMTs is set in a different color. The reference position of each PMT in the DOM is shown in Table A.1

physical studies.[*] The DOM has PMTs disposed in six rows, as represented in Figure 2.5, named from A to F. The bottom hemisphere of a DOM is composed of rows A, B, C, and D with PMTs pointing in downward angles at 180, 148, 124, and 107 degrees respectively with an up-pointing vertical reference. The top hemisphere is composed of only two rows E and F with PMTs pointing upwards in angles of 56 and 73 degrees with an up-pointing vertical reference. This arrangement of PMTs has the purpose of preventing blind spots and provide directional sensitivity. Every single DOM contains a Central Logic Board (CLB) that is the brain of the module, and it performs every logical task for its correct functioning. Some other chip-sets include the power board that distributes and regulates the right voltage for every PMT, and the signal collection board (octopus board) that connects every PMT base to the CLB. Other parts of DOMs include the cooling system that prevents from overheating the internal parts, and the set of the valve, penetrate and pressure gauge.

Additionally, DOMs contain other sensors used for positioning calibration purposes, among these sensors, there are a piezo-acoustic sensor, a digital compass, and an accelerometer. The piezoelectric sensor helps to determine the 3D-position of the DOM in 3D by using acoustic multilateration techniques. The digital compass allows the DOM to know the orientation of each PMT, and the accelerometer is used to determine the tilt, pitch, and yaw of the DOM. These sensors are very relevant because DOMs are displaced and rotated constantly by the influence of sea currents. Another vital equipment that composes the calibration system for light detection includes a nanobeacon and the PMTs that time calibrate every DOM. Each DOM is contained in a protective glass sphere vessel, Vitrovex, thick enough to overcome the tremendous pressures occurring in the bottom of the sea. Vitrovex container is surrounded

---

[*]https://cc.in2p3.fr/
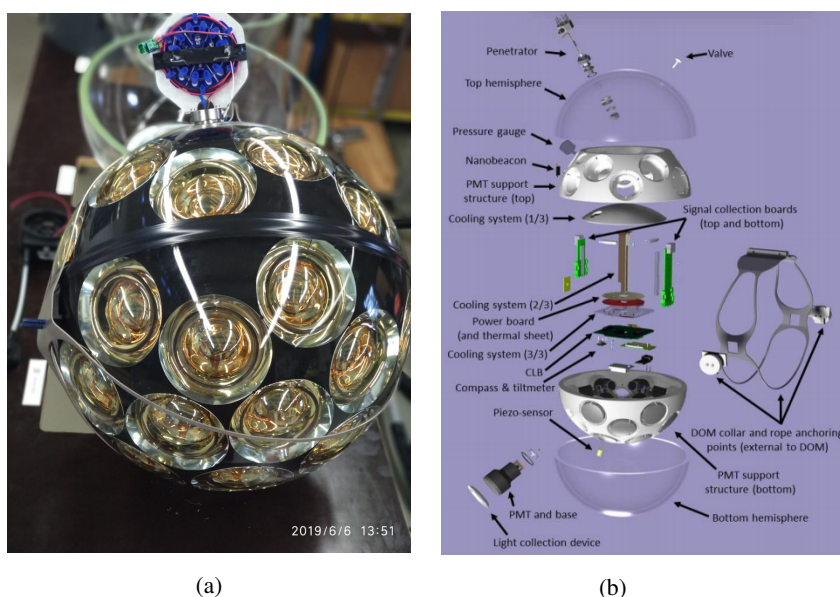
Figure 2.6: Main components of a DOM. (a) Mounted DOM with PMTs disposal clearly visible. (b) Artistic representation of a DOM displaying its main components.

by a titanium collar that helps in the physical interconnection of the DOMs. All the mentioned components can be observed in Figure 2.6[9]. The PMTs convert light into an electrical signal. The technology developed by KM3NeT makes it possible for instrumentation to have minimal cost and maximum reliability. These conditions are essential to cover the largest possible volume of seawater with a 3D spatial array of photo-sensors. The PMTs used in the first phase of KM3NeT are manufactured by Hammamatsu Photonics (model R12199-02) as it combines a relative good quantum efficiency for light in a range of around 375 to 750 nm, with a good timing response and a low price per unit[22]. [†]

Vitrovex: the high pressure-resistant sphere

This is the main component studied in this work, which is assumed to be under the influence of radioactivity of ^{40}K due to its constituent materials. The glass vessel is as important as other vital parts of the detector since DOMs are contained in a 14 mm thick, and 17-inch diameter container, weighting 17.2 kg in air, made of a glass material known as Vitrovex. Vitrovex is a special borosilicate glass used in laboratories, industry, and for specific heavy-duty tasks. It is composed in a 81% of SiO_2, 13% of B_2O_3, 2.4% of Al_2O_3, 3.0% of B_2O_3, 0.6% of K_2O, ^{40}K makes a 0.012% of potassium found in nature and it is the radioactive material with the largest presence in Vitrovex[23]. Although it is not declared in the specifications, Vitrovex also may contain other traces of radioactive materials such as ^{232}Th

---

[†]The technical details of the PMT can be observed in the appendix (Table A.3)

and ^{238}U, which are part of this study. In Table 2.1, it is observable the mass-specific activity of materials contained in Vitrovex. Vitrovex is a high-pressure resistant glass, which is needed to stand extreme pressures found in the depths of the Mediterranean Sea. According to the safety information of the material, it has the physical property to stand pressures of 64 GPa (between 20 to 40 GPa is estimated at the KM3NeT sites). Vitrovex is biologically inert, environmentally neutral, and not soluble in water, which means that it will no contaminate the waters of the sea. In Figure 2.7, a sphere of Vitrovex is observed and the decay of radioactive materials in specific areas of the glass sphere that can randomly occur[23][24].

Mass-specific activity (Bq/kg)				
	VV 1	VV 2	VV vessel	BT vessel	Wacker & QSI gel
214Bi	4.01±0.16	4.29±0.17	8.14±0.20	5.14±0.17	<0.15
214Pb	4.82±0.12	4.83±0.14	8.83±0.18	5.29±0.16	<0.11
234Th	5.2±0.9	4.8±1.2	5.1±0.8	4.7±0.7	<0.76
238U-Chain	4.53±0.10	4.61±0.19	8.42±0.13	5.2±0.12	<0.11
228Ac	1.31±0.09	1.34±0.22	2.37±0.24	1.71±0.22	<0.26
212Pb	1.42±0.10	1.34±0.11	2.03±0.12	1.04±0.11	<0.11
208Tl	1.38±0.20	1.32±0.21	2.06±0.28	1.16±0.25	<0.15
232Th-Chain	1.39±0.09	1.34±0.09	2.27±0.10	1.16±0.09	<0.10
235U-Chain	0.56±0.07	0.61±0.07	0.75±0.08	0.61±0.09	<0.05
40K	53.6±1.7	57.5±1.8	<0.99	1.0±1.4	<1.32
Measurement duration (s)	256419	262815	265731	269667	251533 315285
Sample mass	$(641 \pm 5)g$	$(604 \pm 5)g$	$(4.37 \pm 0.01)kg$	$(4.43 \pm 0.01)kg$	$(649 \pm 5)g$ $(651 \pm 5)g$

Table 2.1: Mass-specific activities from Vitrovex, the average activity of their isotopes is also given. The last row present the weight of the samples respectively from which the data was obtained. VV stands for Vitrovex and BT for Benthos.[18]
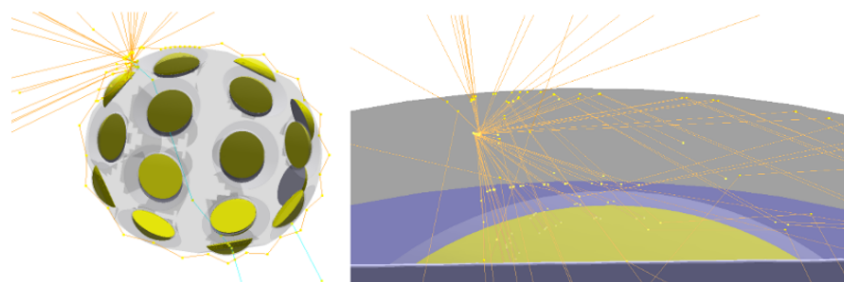
Figure 2.7: Decay of radioactive elements contained in Vitrovex produce emission of light. The decay occurs directly above PMTs with a coincidence detectable signal. Adapted from Reference[24].

2.4 Experimental Challenge: background at the KM3NeT sites

The characterization of ^{40}K optical signatures coming from Vitrovex is important for a better understanding of the optical background at the KM3NeT sites. It is essential that the characterization occurs in a laboratory before the deployment of the DUs in the deep-sea because signals could get mimicked as other sources of background are present. Random background light causes variable hit rates in PMTs, which challenge the discovery of neutrinos. In deep-sea neutrino observatories like KM3NeT, two main types of background are present: one resulting from the physical processes occurring in the atmosphere (physical background), and other occurs from the optical activity of the detection environment (optical background).[5][7]

2.4.1 Physical background

Two types of physical background might reach KM3NeT detectors: one is a "reducible background" produced by atmospheric muons, and the other is an "irreducible background" caused by neutrinos created in the atmosphere. The flux of down-going atmospheric muons is several orders of magnitude higher than the atmospheric neutrino signal as seen in Figure 2.8[7]. Atmospheric muons can travel through the whole atmosphere and reach the detection media causing a track in the detector, inside or outside sensitive volume. These muons created by cosmic rays interacting with the atmosphere can be distinguished from muons produced by neutrinos in the detection medium, this background is reducible and can be done in two ways. The first one is to locate the detectors at significant depths as observable in Figure 2.8, the flux of muons decreases with depth. The second way is to mainly focus on the events detected by PMTs that are looking downwards, where the signal is expected to come from. Additionally, this type of background can be rejected when performing a physical analysis by event selection and proper reconstruction of track direction. This technique consists of restricting the search for the signal of up-going events.[7] The irreducible background relates to the production of muons caused by atmospheric up-going neutrinos when passing through the detection medium. It is called irreducible since there is no physical way to prevent it from happening, not even by looking at up-going events. Although it is physically irreducible, at high energies, the cosmic neutrino flux dominates over atmospheric neutrino background, and so it can be identified by their energy spectrum as observed in Figure 2.8.[7]

2.4.2 Optical background

There are two components of optical background at the KM3NeT sites, one originates from the bioluminescence emitted by micro and macro organisms, and the other caused by radioactive decay of isotopes such as ^{40}K, ^{232}Th, ^{238}U decaying in both the detection environment and in Vitrovex itself. The tracks created by neutrino events can be correlated and detected by many PMTs, however, events created by bioluminescence and radioisotopes such as ^{40}K are random and located in specific areas making that just few PMTs can be able to detect it, as suggested in Figure 2.7[7].
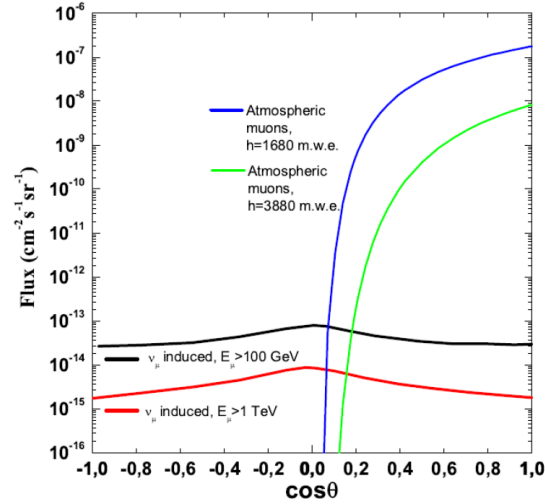
Figure 2.8: Zenith angle distribution for atmospheric muons, and neutrino-induced events. Muons at two different depths and atmospheric neutrino-induced muons at two different energy thresholds are compared. Adapted from Reference [7].

Bioluminescence

Bioluminescence is the production and emission of light by living organisms. It spans all over the oceanic dimensions from bacteria to fish [25]. A vast diversity of marine microbes and animals can generate their light, and in most regions of the ocean, bioluminescence is the only source of light. In the depths of the sea, an estimation of 90% of all deep-sea creatures use bioluminescence [26][27]. The oxidation of light-emitting molecules in conjunction with catalyzing enzymes, usually luciferin mixed with luciferase or another photo-protein, produces bioluminescence. This light appears as the result of energy released during the chemical reaction [25]. Most of light is mainly in the blue region of the visible spectrum, just as the peak wavelength of Cherenkov light coming from neutrino signals [25]. Bioluminescence can be produced frequently along time, generating a baseline of events. Additionally, some spontaneous events, for example, big sea creatures passing through the detector, can produce bioluminescence with high intensity. This behavior can be observed in Figure 2.9 [7]. The intensity of bioluminescence varies depending on the location, within the Mediterranean Sea, a higher activity has been observed in shallow seabeds as one goes towards the west. [26] Considering the location of KM3NeT detectors, ORCA is more susceptible to bioluminescent sources as it lays in a shallower area west than in ARCA.

Radioactive Decay in DOMs

On the other hand, potassium is only one of the many minerals present in seawater but is nevertheless very important for KM3NeT. ^{40}K forms a constant background of events that altogether with bioluminescence forms a baseline as
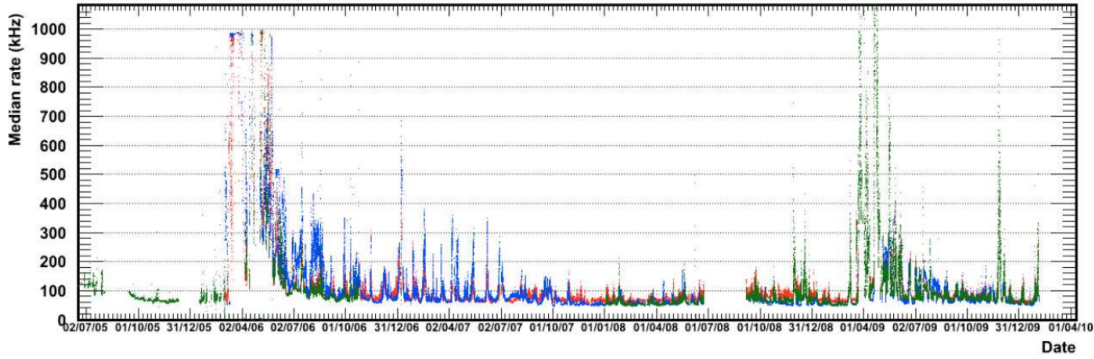
Figure 2.9: Time evolution of the optical background registered by ANTARES, close to KM3NeT-ORCA site. Large peaks represent spontaneous bursts of bioluminiscence caused by sea creatures, ^{40}K and constant bioluminiscence forms a continuous baseline. Adapted from Reference [7].

shown in Figure 2.9. However, ^{40}K is not only present in seawater, but also in Vitrovex of DOMs. ^{40}K has a bigger relevance since it has a larger activity; it is noteworthy and makes up to 0.0117% of the potassium in seawater with an activity of 14 kBq/m^3. ^{40}K has a half-life of 1.25×10^9 years and two possible channels of decay. The most probable channel occurs when ^{40}K becomes ^{40}Ca through β decay, and the second channel occurs when ^{40}K becomes ^{40}Ar through e^- capture [7]:

$$
\begin{aligned}
^{40}\text{K} &\to {}^{40}\text{Ca} + e^- + \bar{\nu}_e && (89.3\%), \\
^{40}\text{K} &\to {}^{40}\text{Ar} + \nu_e \to {}^{40}\text{Ar} + \gamma && (10.7\%).
\end{aligned}
\tag{2.10}
$$
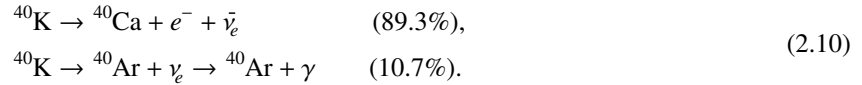
In the first channel, an electron with an energy of about 1.3 MeV is produced, meanwhile, in the second channel photons with an energy of about 1.46MeV are produced. In both cases, energy is enough to generate Cherenkov light as the Cherenkov threshold in water is about 0.25 MeV. [28] Since KM3NeT DOMs can detect several photons from a single ^{40}K decay, this makes the isotope of potassium suitable for time calibrations between PMTs in a DOM. From the other radioactive materials present in Vitrovex, it is worthy of mentioning ^{232}Th, and ^{238}U as these are considered in the simulations of KM3NeT. ^{232}Th is the most common isotope of thorium found in nature, it has a half-life of 1.405×10^{10} years, its channel of decay is through ^{228}Ra by α-decay, it is, ^{232}Th $\to$ ^{228}Ra $+ \alpha + E$. ^{238}U is the most common isotope of uranium found in nature. ^{238}U has a half-life of 4.468×10^9 years, and its decay channel is through ^{234}Th by α-decay, it is, ^{238}U $\to$ ^{234}Th $+ \alpha + E$. The energy released during decay is 0.273 MeV, distributed among the particles, which is also above the Cherenkov threshold in water.

In this work, the focus of study is the background events caused by ^{40}K, contained in the Vitrovex that protects the KM3NeT DOMs. It is essential to understand the rate generated by ^{40}K in order to well identify the source of emission, Vitrovex or seawater, aimed to better characterize correctly the optical background during KM3NeT operations.

Chapter 3

Experimental Methodology

In this chapter, the construction of the experimental set-up for reaching the objectives of this work is presented. The data taking routine and the analysis plan are described as well, and the particularities of each data sample are also given. All the methods, protocols, and models used in the experiment are introduced and explained.

3.1 Test Bench

In Figure 3.1, the experimental set-up used to evaluate the ^{40}K contribution from the Vitrovex of the DOM can be observed. This was set up at Nikhef (Amsterdam). It consisted of a DOM connected to a power supply, interconnected to a central PC through a white rabbit switch[29]. The DOM is located inside an aquarium, supported by a metallic structure, and secured to the bottom of the container. The aquarium housing the DOM, in turn, is inside a Dark Box (optical shielding), which isolates from any external source of light. The dark box has a particular design of an electrical wire gutter that connects the DOM (inside of the dark box) with the white rabbit switch and to the power supply (outside of the dark box). This gutter was designed with many corners inside to prevents light from entering the dark box. Data acquisition is synchronized to the nanosecond level by the white rabbit switch and sent storage in a PC. Data is transmitted from the DOM, all the way to the PC through optical fibers which provides timing synchronization and a transfer speed of up to 1 Gb/s . Splitter modules are located in the optical fibers path, one is between the DOM and the white rabbit switch, and the other between the switch and the PC as observed in Figure 3.1. The white rabbit switch synchronizes the collection of data by the detector with the monitoring system in the PC, this precise synchronization is possible thanks to the absolute nanosecond timing protocol proper of the switch. The PC controls and monitors the data from the DOM with a set of customized software developed by KM3NeT.
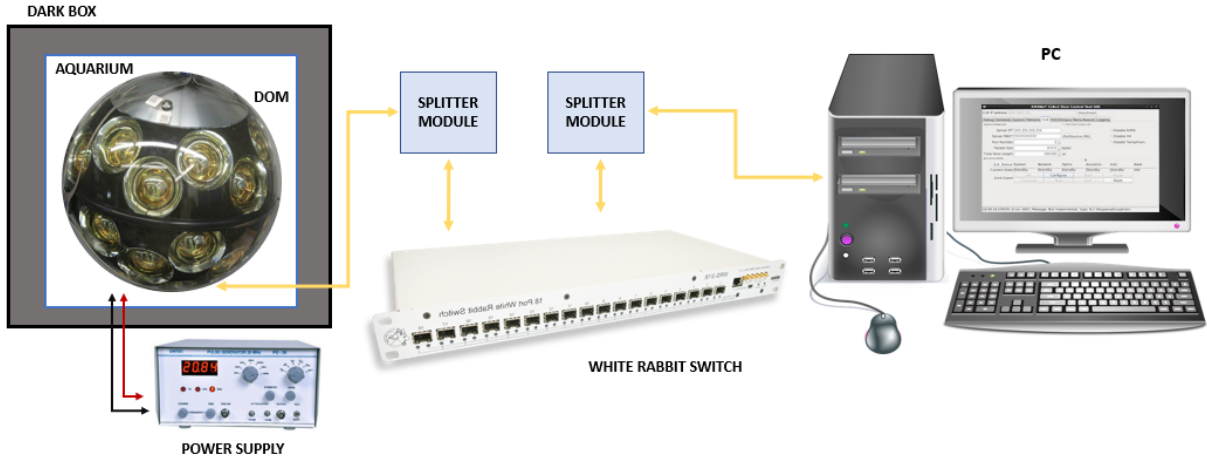
Figure 3.1: Experimental test bench used to evaluate the contribution of ^{40}K from Vitrovex in this work.

3.2   Data Acquisition

`CLBv2_Remote` is the first software package used, it allows to control the DOM's CLB options and features. It is suited with a Graphical User Interface (GUI) that let choose between different acquisition options. In order to control the CLB with the software, the first stage is to establish a connection between the CLB of the DOM with the PC by assigning the IP address of the CLB. This software allows to configure the so-called Octopus Board (multi-PMT merger), by allowing to select which PMTs will be used. At this stage the PMT B1 had to be turned off since it was not working properly in the DOM used for the experiment.* Once the IP is assigned and the Octopus Board configured, the communication establishes between the DOM and the PC. Then the software used to monitor the events detected by every single PMT of the DOM in real time is `CLBSwissknife`. Finally the code used to record data was based on `JPP` software packages, KM3NeT official software, this not only allows to record data but also to analyze it since it is a set of interfaces, classes, and methods inspired in `Java` and written in `C++`[30]. `JPP` provides many useful resources as language-specific auxiliary classes and methods, multi-dimensional interpolation methods, muon energy loss methods, neutrino interaction cross-sections, 2D and 3D geometry packages, and much others. For this experiment only the `JPP` package configurations for time calibration and coincidence levels were used.

White Rabbit Switch

It is an 18-SFP port switch, as the main element of a white rabbit network, and it was designed as part of the White Rabbit Project. It was initially developed as a tool for timing system of experimental high energy physics facilities. The White Rabbit Switch (WRS) hardware is licensed under CERN, its firmware and driver software are available as open licences.[29] A WRS works under the White Rabbit protocol which provides nanosecond accuracy and

---

*In Table A.1 it can be observed the list of PMT id and their corresponding PMT channel.

picosecond precision of synchronization. White Rabbit allows precision time-tag measured data and let triggering data taking in large installations at the same time by using the same network to transfer data. These features of white rabbit protocol are used by KM3NeT for PMT synchronization and data collection systems in a 1 ns time window. Figure 3.2 pictures the uses of a WRS, showing how one master WRS can synchronize others until reaching the target activity.
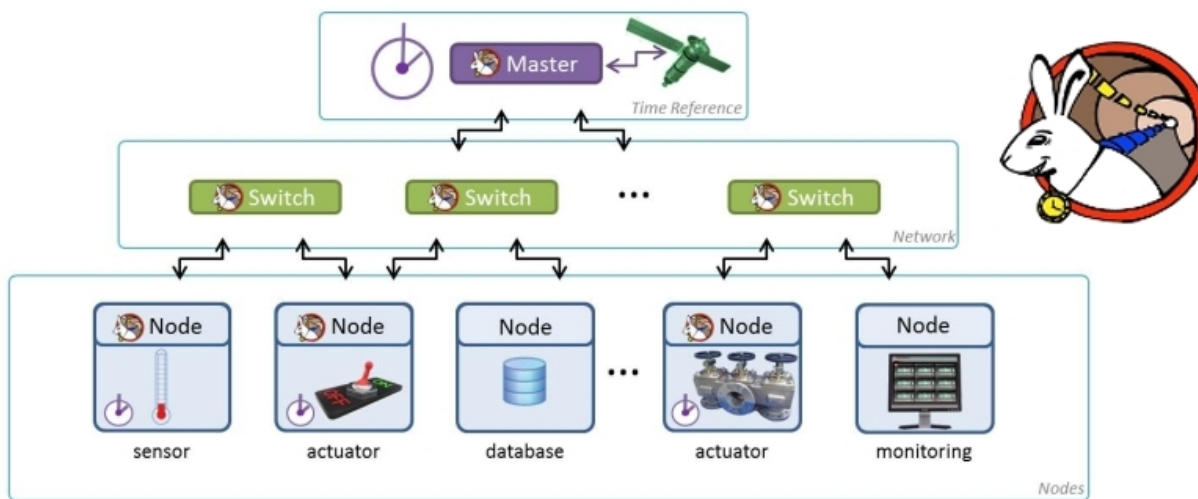
Figure 3.2: Scheme showing how White Rabbit works, and the available features and uses. Adapted from Reference[31]

Data Taking Routine

The aim of this work is to study the rate caused by ^{40}K in Vitrovex. To perform this, a data taking routine was designed with four configurations of the test bench. Two of them consisted of the DOM in air as the medium of detection, and the other two configurations had the DOM submerged in tap water to mimic the *in-situ* operation. Additionally, one configuration in each medium of detection included the DOM covered with a thick polyethylene plastic bag of around 250 to 1000 micrometers thick, as an isolation method. The physical configuration of the DOM for each test bench is shown in Figure 3.3. The experimental settings for all data taking routines were basically the same, each configuration was recorded during 1800 seconds, and at each different configuration, a recovery time for the PMTs was necessary. This had the purpose to stabilize the dark count rate proper of the PMT, and depended on the initial exposure of light. The target was to reach the lowest possible rate in the dark. The objective was to get around 5000 to 6000 hits per second[22].

In the Setup N1, (Figure 3.3a), the DOM is located in an aquarium with no water, inside the dark box, no isolation is applied. The black plastic bag does not cover the DOM, so the possible sources of light are expected to include ^{40}K decay coming from the Vitrovex of the DOM (and maybe coming from the glass walls of the aquarium), as well as

(a)   (b)

(c)   (d)
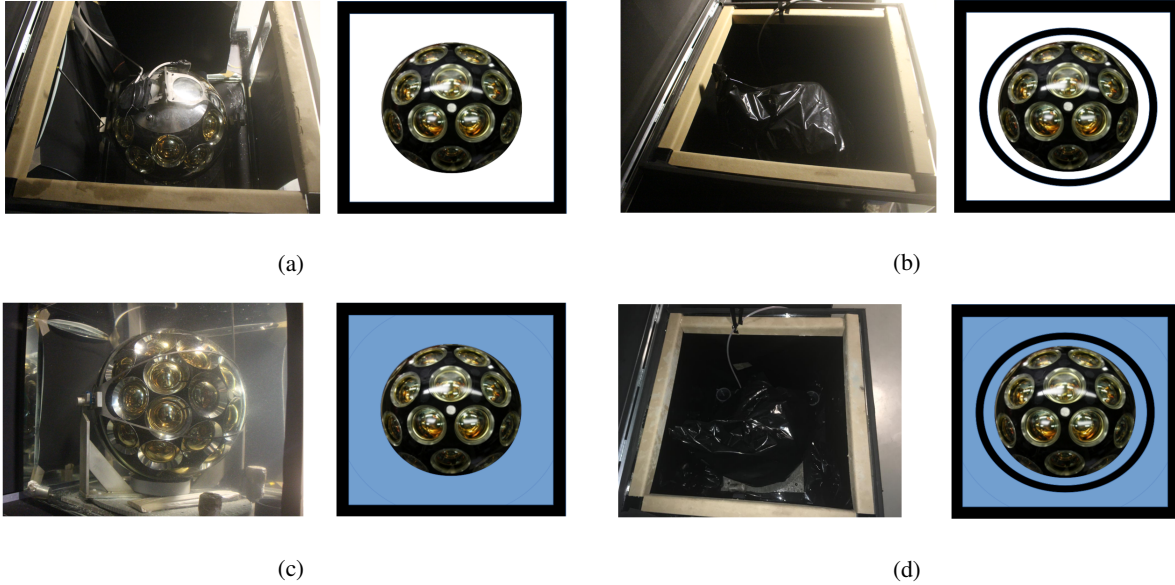
Figure 3.3: Setup of the data taking routine. The black circumference around the DOM represents the plastic bag used as isolation. (a) Setup N1: `no_water_no_bag`. (b) Setup N2: `no_water_with_bag`. (c) Setup N3: `water_no_bag`. (d) Setup N4: `water_with_bag`.

down-going atmospheric muons passing through the medium. In the Setup N2, (Figure 3.3b), the DOM is located in an aquarium with no water, inside the dark box, isolated by a black plastic bag. The possible sources of light are expected to be ^{40}K decay coming from the Vitrovex of the DOM and reduced count of ^{40}K decay coming from glass walls of the aquarium, and a lower chance of down going muons. In the Setup N3 (Figure 3.3c), the DOM is located in an aquarium filled with water, inside the dark box, with no isolation, the black plastic bag does not cover the DOM. The possible sources of light may include ^{40}K decay coming from the Vitrovex of the DOM (and maybe coming from the glass walls of the aquarium), and down-going muons produced in water or produced in the atmosphere. In the Setup N4, (Figure 3.3d), the DOM is located in an aquarium filled with water, inside the dark box, isolated by a black plastic bag, only to detect light produced by the DOM itself. The possible sources of light in this case might include ^{40}K decay coming from the glass sphere of the DOM (and maybe coming from the glass walls of the aquarium), and down-going muons passing through the glass.

3.3   Data Analysis

The collected data is analyzed by implementing `JPP` software package. Two software routine codes were used as illustrated in Figure 3.4. By using the first routine, time calibration, the rate in Hertz caused by the detection of

correlated events from the range of PMT-pairs of a DOM in a certain time window is obtained. Every routine step contains a set of extra available options that can be used depending on the needs. The steps used in this first routine are explained as follows:

- `JCalibrateK40`: it is used to process data that contain correlated events produced by sources such as ^{40}K in or around a DOM. The result of running this code is a 2D histogram containing the time differences between hits † from each unique PMT-pair in that DOM. PMT-pairs are obtained from a combination,

$$C_r^n = \binom{n}{x} = \left(\frac{n!}{x!(n-x)!} \right). \tag{3.1}$$

  In total, for a DOM with $n = 31$ PMTs, there are 465 unique pairs ($x = 2$) since $(31 \times 30)/2 = 465$. A higher number of PMT-pairs means higher possibility of smaller angles between PMTs. At the same time, the random background and live time of each PMT pair are monitored using separate 1D-histograms. By default configuration, the calculation of the background is based on the probability of random coincidences using the measured singles rates obtained from the summary data.[32]

- `JMergeCalibrateK40`: takes the output of `JCalibrateK40` and makes a single histogram with the normalized coincidence rates of each PMT-pair. It is possible to convert multiple outputs of `JCalibrateK40` at the same time.[32]

- `JFitK40`: it fits a model to the output histograms of `JMergeCalibrateK40`. This model is based on the coincidence rate as a function of the opening angle between the axes of a pair of PMTs.[32]

- The last step of the time calibration routine is the Rate Integration, which includes a self made code used to integrate over a 2D histogram produced from the first three steps.

The second routine used, the level of coincidence, ends up showing the coincidence rate in Hertz based on a specific amount of PMTs detecting an event in a defined time window. In the same way as the time calibration routine, each routine step contains a set of additional options that can be used as needed. The steps used in this second routine are explained as follows:

- `JMonitorMultiplicity`: it is a complementary program to analyze coincidence multiplicity (as explained shortly below). It will evaluate the time difference distributions for the different multiplicities.

- `JFitMultiplicity`: it is a complementary program to fit multiplicity rates from `JMonitorMultiplicity` output. A histogram showing a gaussian of the time difference versus events, for each multiplicity, is produced. Additionally, two histograms summarizing the rate from the gaussian of each multiplicity are created, where the background of uncorrelated events has been subtracted. One of the histograms is based on inclusive multiplicity, which means that it contains the sum of rates for multiplicities above the displayed level, for example, an inclusive M = 2 will contain the rate for M = 2 up to 31 . For the other histogram, the rate is exclusive to the showed multiplicity.

---

†Combined data of arrival time and charge information of the signals from the PMTs, recorded as single photon-electron or complete waveform.
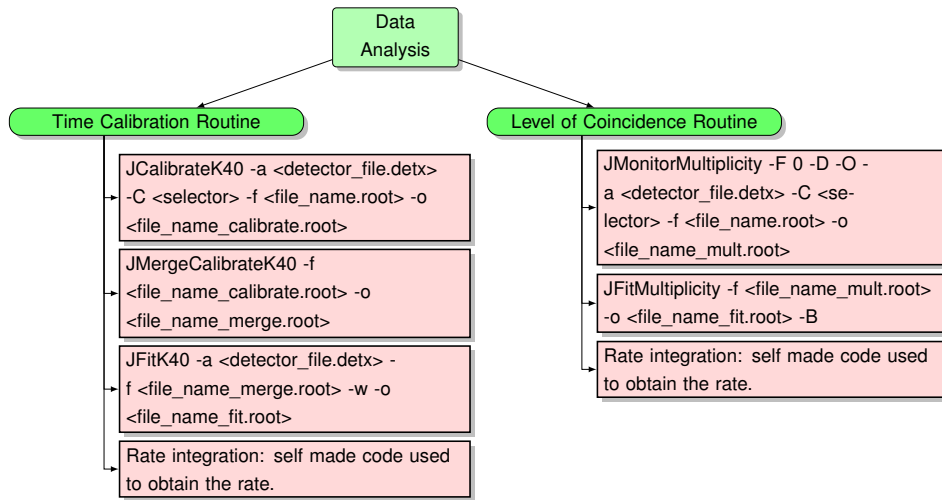
Figure 3.4: Logical sequence showing the two routines used to analyze the experimental data. Steps describing each routine are specified as well.

- The last step of the level of coincidence routine, the Rate Integration, is a self made code used to integrate over an 1D histogram and to obtain a numerical value which will be summarized in tables in Chapter 4.
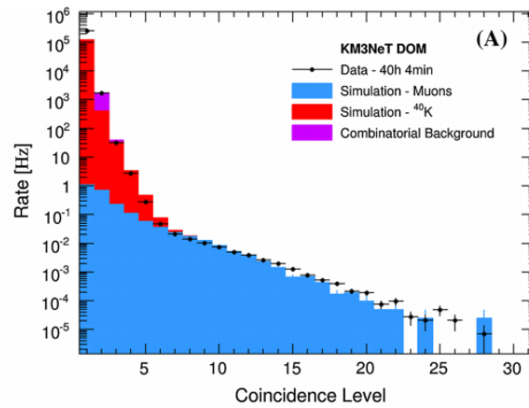
Figure 3.5: Histogram of a simulation that shows that ^{40}K activity is better detected at low coincidence level or multiplicities. Adapted from Reference[1].

^{40}K Coincidence Analysis

As explained before, the time calibration between PMTs of the same DOM is implemented. This intra-DOM calibration refers to the calibration of the relative time offsets of PMTs in a DOM. In the sea, PMTs would detect the

background coming from several sources, including the ^{40}K decay in seawater, but since the experiment developed for this thesis uses tap water and a better controlled environment, the ^{40}K source gets restricted only to Vitrovex, as possible. As mentioned earlier, ^{40}K decay releases β particles able to induce Cherenkov light in a vicinity that can be detected only by a few PMTs. Cherenkov photons can create a time coincidence of two or more hits in the DOM, as represented in Figure 2.7.

Since the ^{40}K decay contained in the Vitrovex occurs at certain spots of the DOM, only a few PMTs will see the occurring event at the "same time". It is essential to know the concept of Coincidence Level or Multiplicity (M), which is defined as the number of PMTs in a DOM detecting a photon within a time window of 10 ns. For events caused by particles traversing throughout the detector , many PMTs of a DOM will see the event, resulting in a high multiplicity, typically M > 6. Events occurring in particular spots of the Vitrovex, will be observed only by few PMTs, usually between M = 2 or 3. This information is described in the simulation at Figure 3.5.

Chapter 4

Results & Discussion

This chapter presents the results obtained from experimental setups described in the previous chapter, with the purpose to find the rate produced by radioisotopes contained in the Vitrovex, more specifically the ^{40}K contribution. A discussion is presented with the purpose to compare the simulation made by KM3NeT, fitting the best conditions as possible to the results obtained by the experimental results of this work. Results were posted periodically at the GitHub [*] of KM3NeT in order to make it open available. Simulations are stored at the ELOG [†] webpage of KM3NeT [33].

4.1 Coincidence Rates by ^{40}K

This study considered both analysis routines, time calibration and level of coincidence, with specific configurations. The settings for `JCalibrateK40`, first stage of the time calibration routine, were configured with a specific time window of 15 nanoseconds (`-T 15`) an exclusive multiplicity of two (`-M "2 2"`), a definition of background established from 10 to 15 nanoseconds (`-B "10 15"`), and a selection of background based on random coincidences (`-b randoms`). By using a small multiplicity, it allows for higher reliability of events occurring in particular sections of a DOM. The time window, more prominent that the definition of multiplicity based on 10 ns, allows for better identification of the background in a gaussian distribution of events based on time differences. The events considered as background are the ones produced by uncorrelated coincidences, which create a "constant floor" of events. After running `JCalibrateK40`, the rates for correlated events are obtained. The histogram showing these rates for experimental data, and for each experimental set up can be seen in Figure 4.1a. This histogram presents a relation between the rate and each number of PMT-pairs. It was obtained after the integration over the time differences of a 2D-histogram produced by the time calibration routine. The 2D-histogram contain events related with the PMT-pairs and the time at which they were detected, in a time window of 15 ns. A larger number of PMT

---

[*] Link to the issue of the GitHub: https://git.km3net.de/simulation/omgsim/-/issues/3#note_16151

[†] Link to the ELOG repository:https://elog.km3net.de/Analysis/519
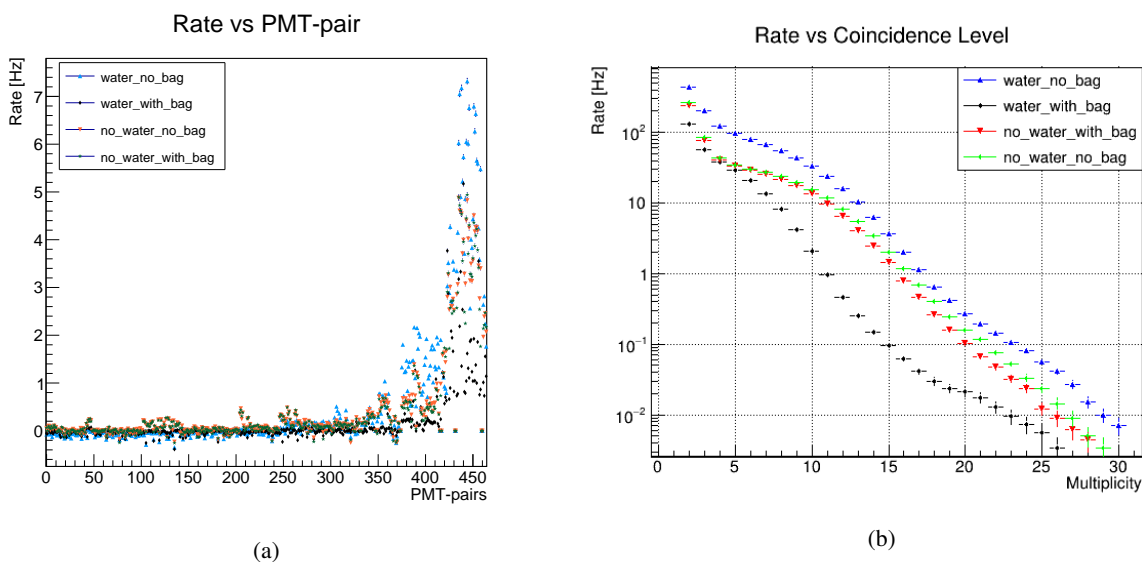
Figure 4.1: Rate for correlated events. (a) Rate vs PMT-pairs obtained with `JCalibrateK40`, the time calibration routine. (b) Rate vs level of coincidence, obtained with the level of coincidence routine, `JMonitorMultiplic-` `ity`.

pairs represent a higher number of possible combinations and includes smaller angles between PMTs. The results of the rates per PMT-pair produced with `JCalibrateK40` routines can be observed in Figure 4.1a and is summarized in Table 4.1, together with results obtained from Figure 4.1b.

By running `JMonitorMultiplicity`, the first stage of the level of coincidence routine, a histogram relating the detected rates with a certain level of coincidence or multiplicity is obtained. From Figure 4.1b, it can be observed that the results with the highest and lowest apparent rate are the ones occurring in water, meanwhile, the measurements in air stay in the middle. The histograms are constructed by the integration of normal distributions for events occurring at a specific time window for every multiplicity level. The background of random coincidences is calculated individually for every degree of multiplicity. As an example of how the background of random and uncorrelated events is subtracted from the actual rate, the Setup N4 is used, as the results display the lowest detected rate. When detecting correlated events, with a certain degree of multiplicity, the occurrence will fall in a time window of 10 ns. The events that do not have a correlation, which can be random events, will appear outside the window of multiplicity, forming a kind of "floor" of background. In the Figure 4.2a, it can be observed the events in a window of time of ±10 ns, and how tails of the distribution start to converge to a constant rate. In the Figure 4.2b, the window of time has been enlarged to ±15 ns, so that it can be better studied, clearly showing the "floor" of uncorrelated events. To obtain the rate of ^{40}K signals, the area of the Gaussian distribution, for each

Configuration	JCalibrateK40 [Hz]	JMonitorMultiplicity [Hz]
Setup N1 (`no_water_no_bag`)	196.949	179.178
Setup N2 (`no_water_with_bag`)	185.413	166.426
Setup N3 (`water_no_bag`)	239.894	241.597
Setup N4 (`water_with_bag`)	69.326	74.347
Simulation	69.266	-

Table 4.1: Integrated rates obtained from the data of the four experimental setups, showing the expected reference rate of the simulation for the activity of ^{40}K in Vitrovex. In absence of ^{40}K from seawater, the detected rate might be associated with the experimental setup.

multiplicity, has to be integrated, and the constant floor subtracted. The produced rate, for each multiplicity, is inclusive; which means that the events will correspond to an equal and higher than the degree of multiplicity showed. If the procedure described above is performed for a M = 3, the rate will include events corresponding to M = 3 to 31. In the other hand, rates can also be exclusive. This rate is obtained in the following way: if we have two gaussian distributions, each representing an inclusive rate, one with M = 2, and other with M = 3, each will have to be integrated and its constant background subtracted . After this, the M = 3 will have to be subtract from M = 2, obtaining the value of the exclusive rate for a M = 2. The exclusive rates for the different configurations of the setups are presented in Figure 4.3a. The focus of this plot is to show the rates at low multiplicities, and as it can be seen, M = 2 has the most significant rate in every measurement. Larger multiplicities present not rate at all since uncorrelated rates were subtracted, and at a larger multiplicity, there is a smaller probability to have correlated events.

The experimental results obtained by the analysis routines along steps are summarized in Table 4.1 can be compared with the simulation, which include the events produced by ^{40}K in Vitrovex. Two histograms showing the rate per PMT-pair for the simulation of ^{40}K can be observed in Figure 4.4. This simulation is analyzed with the time calibration routine as it was designed to simulate the radioactive decay of ^{40}K. The configuration of this simulation uses a time window of 24 nanoseconds (`-T 24`), establishes a rate range of up to 15000 Hz (`-V "0 15000"`), and includes count events occurring in all multiplicities up to 31 (`-M "2 31"`). The biased coincidence rate for this simulation is shown in Table 4.1 (last row).

For a refined comparison with the simulation, only the data from the Setup N4 is considered since it presents the lowest amount of background sources and the lowest detected rate. The configuration of the simulation for `JCal-ibrateK40` includes the options: `-T 24`, `-V "0 15000"`, and `-M "2 31"`, meanwhile, the configuration of the experimental data includes the options: `-T 15`, `-M "2 2"`, and `-B "10 15"`. For this case, the rate obtained with the time calibration routine (`JCalibrateK40 M"2"`) is 69.33 Hz, meanwhile, the rate obtained by the level of coincidence routine (`JMonitorMultiplicity M"2"`) is 74.35 Hz. By comparison with the simulated data which suggests a rate of 69.27 Hz, it seems that the estimation in this work is close to that expected. The difference in rates could be caused by any additional background that was not eliminated entirely nor identified,
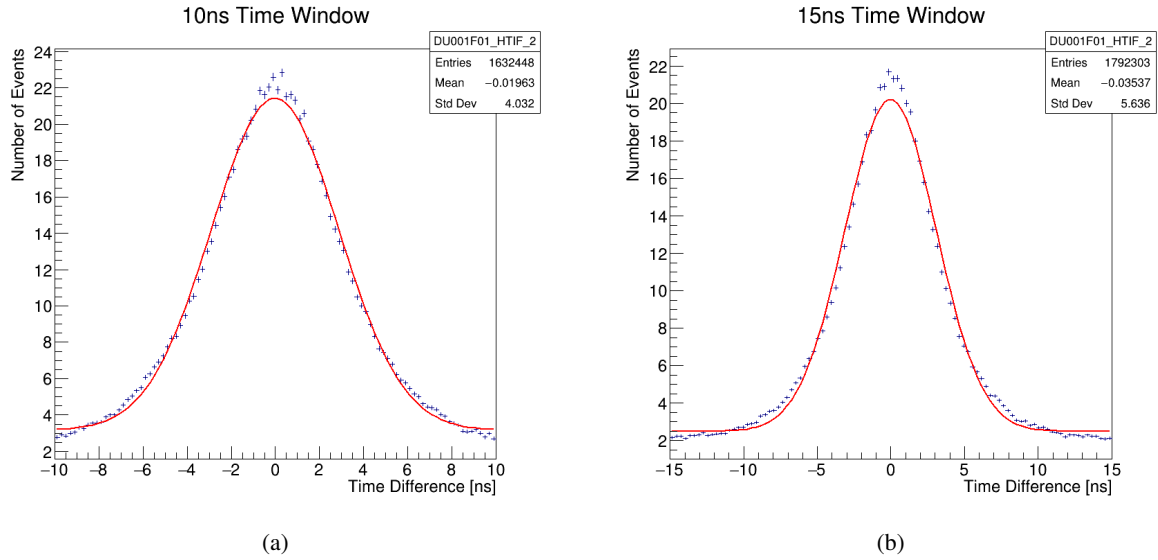
Figure 4.2: Gaussian distribution for a M = 2 for Setup N4, `water_with_bag`, showing the background of uncorrelated events as it forms a constant floor. Blue marks represent real data, meanwhile the red line corresponds to the gaussian best fit. (a) Time window of 10 ns. (b) Time window of 15 ns. Notice that both plots do not have the same scale, however observations are valid.
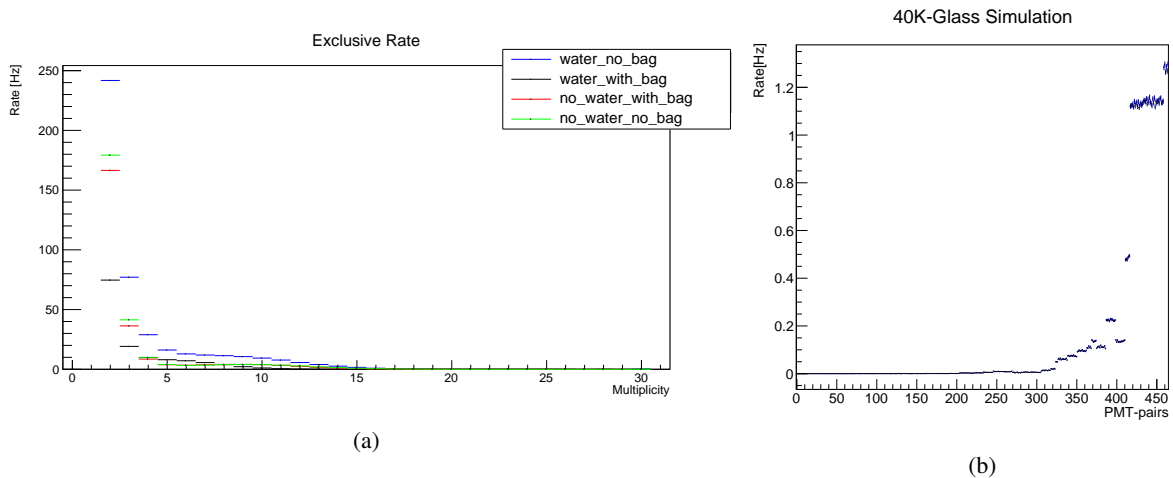
Figure 4.3: Exclusive rates (experimental) and ^{40}K simulation signal. (a) Histogram showing the exclusive rates of the four test bench configurations performed in this work. Small multiplicities show higher rates, meanwhile larger multiplicities present no rate at all. (b) Histogram for the rate vs PMT-pairs for ^{40}K decay in Vitrovex (simulation)[33].
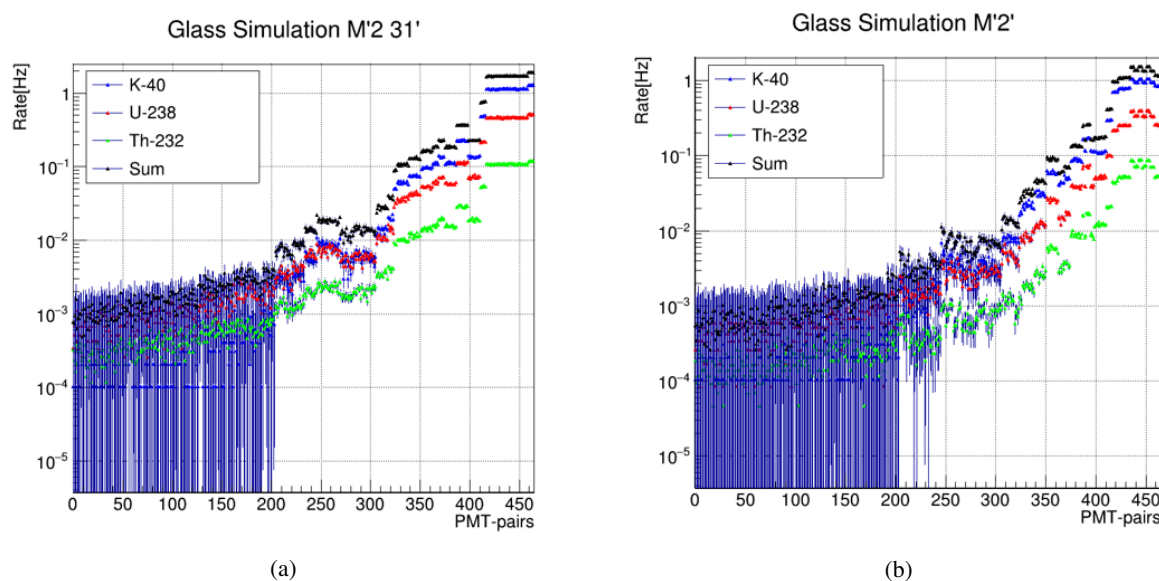
Figure 4.4: Plots of the simulation of radioactive materials in Vitrovex, showing the rate per PMT-pair. (a) Plot for a level of coincidence M = 2 to 31. (b) Plot for a level of coincidence of M = 2.

for example, induced by down-going atmospheric muons. Although this first approach seems to be good because of the close similarity in results from the experimental and simulated data, it is not accurate enough. The first relevant discrepancy appears in the way that data is analyzed with the time calibration routine.

The results from the experimental and simulated data are found very similar by using the parameters with the closest processing options available. For both routines, the parameters that gave the closest results were tested by hand instead of using the exact same parameters applied in the analysis of the simulation. The impossibility for exact reproducibility is because at the time of performing the data analysis, the information of the exact parameters used in simulation was not available. Another point to consider is that the rate produced by radioisotopes in Vitrovex is not unique to ^{40}K, and it may include the effect of small additions caused by more isotopes. For these reasons, a more precise analysis is needed, which is described below.

4.2 Analysis of Radioisotopes from Experimental and Simulated Data

A simulation of radioisotopes as constituens of Vitrovex is available in KM3NeT, designed through Optical Module Geant4 simulation (`OMGsim`) which provides an easy to use simulation of the DOMs containing multiple PMTs, and test radioactive materials in the glass and their activity. As part of a more precise approach, the simulation will consider ^{40}K, ^{232}Th and ^{238}U. The data analysis of the simulation is performed with `JPP` software package and is obtained with the following configuration of `JCalibratek40`: `-T 24 -V "0 15000" -M "2 31"` and

`-M"2"`.

In Figure 4.4, it can be observed the rate produced for each of the three simulated radioisotopes per PMT-pair response. The black line represents the sum of all rates produced by the decay of the radionuclides. Two plots are displayed, the Figure 4.4a corresponds to the rate with a level of coincidence from M = 2 to 31 , and the Figure 4.4b corresponds to rates with a level of coincidence of M = 2 only. After the time calibration and the level of coincidence routines are performed, the main results obtained can be summarized as done in Table 4.2. Notice that for both multiplicity cases, the highest rate belongs to ^{40}K, as expected since it is the radioisotope with the largest mass-specific activity, as showed in Table 2.1 for Vitrovex.

Simulation Rate [Hz]		
	-M"2 31"	**-M"2"**
^{40}K	69.891	51.2442
^{232}Th	30.4883	18.2762
^{238}U	7.40547	3.93436
Total	107.78477	73.45476

Table 4.2: Simulated rates [Hz] obtained from the radioisotopes found in Figure 4.4, for two different multiplicities.

In this analysis, the time calibration routine and level of coincidence routine are used as well for evaluating the experimental and simulated data. In this case, the level of coincidence routine was applied first, via `JMonitorMultiplicity (-F 0 -O -D)` . The option `-F` shows the filtering level, in this case, raw data is used, so the value is zero (`0`). The option `-O` is to monitor occupancy, this produces 2D PMT vs multiplicity plots, and the option `-D` makes a 2D model for the background subtraction. For experimental data, in Figure 4.6, the rate detected by each PMT can be observed. Figure 4.6a shows that the PMTs of a full DOM observe events in a range from 10^5 to 10^7 Hz. PMTs in the top hemisphere (row E and F) detect a slightly higher rate of events compared to the PMTs at the bottom hemisphere (rows A, B, C and D). The rate recorded in water shows the largest values for most PMTs in the test bench that uses no isolation (Setup N3), and the smallest values for the configuration that does use isolation (Setup N4). The rate detected for the measurements in air (Setup N1 and Setup N2) have values just between the maximum and minimum as also concluded in previous section based on Figure 4.1. The Figure 4.6b shows data recorded only for PMTs of the top hemisphere of the DOM, for Setup N4 (`water_with_bag`), the one with the smallest rate from all configurations.

As just mentioned, in Figure 4.6a it is observable that PMTs, looking upwards, in the top hemisphere (rows E, F) show a higher rate. A probable reason for this is because of an optical background induced by down-going atmospheric muons. Since these muons travel in a downward trajectory pointing perpendicularly to the Earth, the PMTs looking upwards might be the ones observing the produced light before it faints. A lower rate is observable for PMTs looking downwards, in the bottom hemisphere (rows A, B, and C), that might include scattering of light from muons or other light sources. The D row which presents the lowest rate for most of the PMTs, it appears

Experimental Rate [Hz]		
Configuration	**-M"2 31"**	**-M"2"**
Setup N1 (no_water_no_bag)	2515.85	450.379
Setup N2 (no_water_with_bag)	2255.32	419.19
Setup N3 (water_no_bag)	4885.47	434.951
Setup N4 (water_with_bag)	1062.82	185.539

Table 4.3: Table that summarizes the rates [Hz] obtained in the analysis of experimental data found in figure 4.7

that most reflections of light caused by a background of muons (if case) do not reach this row. Table A.1 in the appendix section summarizes the positions and angles of each PMT of the DOM used in the experiment. As we move to PMTs in the center of the DOM, the rate decreases as the background caused presumably by down-going atmospheric muons reaches this region with less intensity. *For this reason, the second most important conclusion of this work, the larger rate recorded by PMTs in the top hemisphere of the DOM may be associated with external sources, suspected to be down-going atmospheric muons induced events, however this must be further supported.*
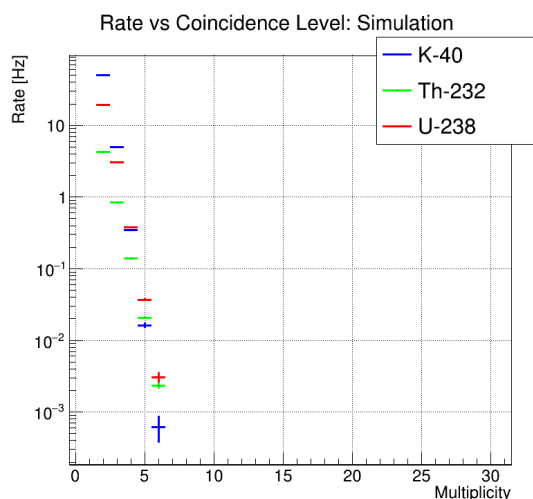

Figure 4.5: Histogram showing the level of coincidence for MC data.[1]

Based on Figure 3.5, it might guess that the radioisotopes effect appear for M < 6, above this, most effects are caused by muons. From Figure 4.1b, it is observable that for M > 6, the rate is really high compared with the simulation found in Figure 4.5, where for M > 6, no events are considered since this analysis is optimized for events induced by radioisotopes composing Vitrovex. *This observation supports conclusions above on the regard that discrepancies might be caused by a source of background not rigorously described in the simulation, and linked to the fact that experimental data interpretation is limited to the particular conditions used in the different setups.* The measurement that approaches the most to the simulation is data collected from Setup N4 (`water_with_bag`) which was shielded to prevent effects caused by other sources of light. Although this measurement is much closer to the simulation, there is still additional influence caused by other suspicious background sources.

Either for experimental and simulated data, time calibration routine was used in order to correlates events by using unique PMT-pairs, under `JCalibrateK40 -T 24 -V "0 15000" -M "2 31"` and `-M"2"`. Moreover, the settings are the same used in both cases in order to further tackle limitations commented in previous section. Results for experimental data are presented in Figure 4.7. Figure 4.7a includes all events observed M = 2 to 31 PMTs at the same time; the rate for this plot ranges 0 to 10^2 Hz. In turn, Figure 4.7b shows that measurements of all setups are

(a)   (b)
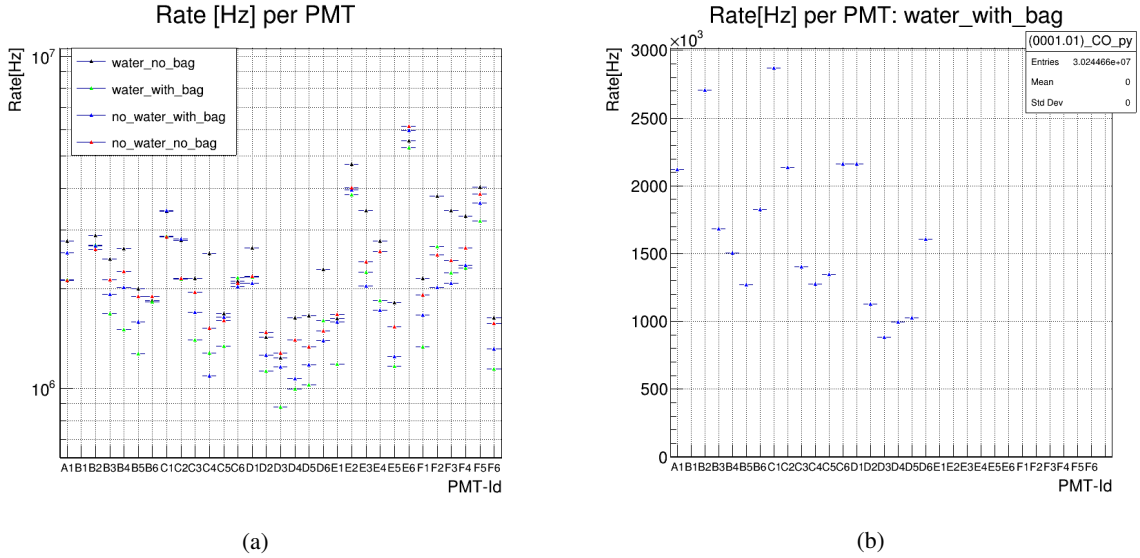
Figure 4.6: Histograms showing the rate per PMT in the DOM (scales are different). (a) Plot showing the events detected by each PMT in both hemispheres. (b) Plot showing the rate detected by each PMT of the bottom hemisphere.
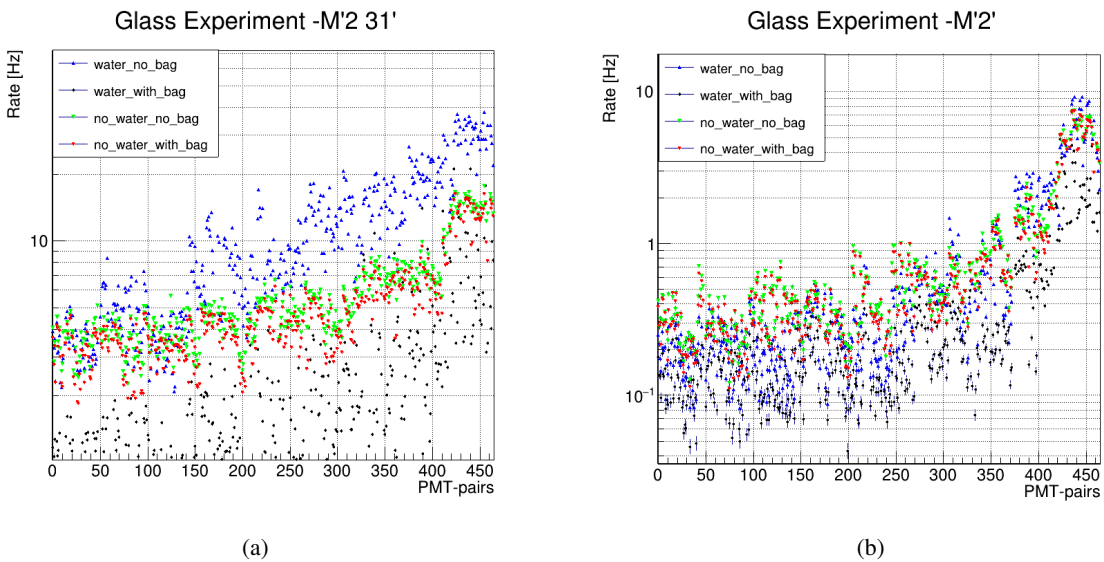

(a)   (b)

Figure 4.7: Plots of the experimental data showing the rate per PMT-pairs. (a) Plot for a level of coincidence M = 2 to 31. (b) Plot for a level of coincidence of M = 2.
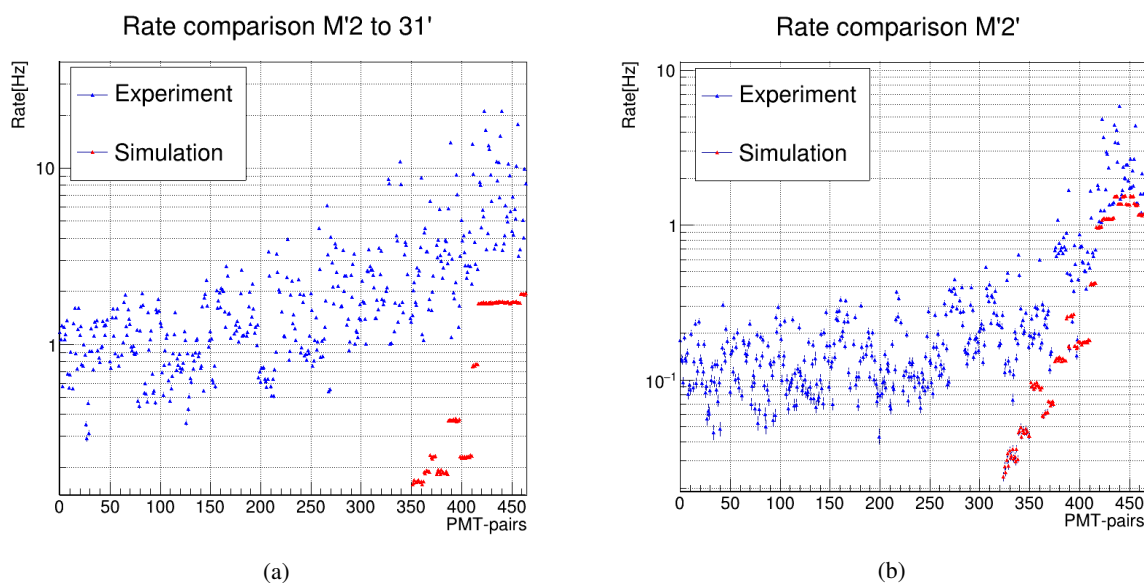
Figure 4.8: Comparison of correlated rates between the simulation of radioisotopes and the experimental data with the Setup N4 (`water_with_bag`). (a) Level of coincidence M = 2 to 31. (b) Level of coincidence M = 2.

closer between them with a rate up to 10 Hz. For both plots of Figure 4.7 the Setup N4 (`water_with_bag`) shows the lowest rate, supporting observations along this chapter. In 4.7a, the Setup N3 (`water_no_bag`) shows the highest rate, whereas the data from the Setup N2 (`no_water_with_bag`) and Setup N1 (`no_water_no_bag`) stay between the maximum and minimum rates. In 4.7b three measurements share a similar rates: Setup N3, Setup N2, and Setup N1. The total rate obtained from the integration over the PMT-pairs was summarized in Table 4.3 before. Additionally, it can be noticed a considerable reduction in experimental rate as events from M = 2 to 31 get neglected in M = 2. By reducing to M = 2, experimental rates get much reasonable among them, this could be an indicator that a constant source(s) produce the correlated rates. Again, Setup N4 is the one that better describes expectations from simulations. Although there are more radioactive materials contained in the glass as shown in Table 2.1, the comparison considers the rate produced only by ^{40}K, ^{232}Th, and ^{238}U as these are the most representative sources causing optical background.

Figure 4.8a shows the comparison for a coincidence level with M = 2 to 31. For this case, the experimental rate is 1062.82 Hz, meanwhile, the rate of the simulation is 107.78 Hz. In Figure 4.8b the comparison includes M = 2, this shortens the possibility of having random coincidences, for this case the experimental rate is 185.53 Hz, meanwhile the rate of the simulation is 73.45 Hz. A significant difference appears in rate when the exclusive level of coincidence M = 2 is applied. A permanent background seems to be still present, however, by restricting the multiplicity, the experimental data and the simulation gets more compatible. In Figure 4.8a, none of the PMT-pairs are close enough but in the Figure 4.8b some pairs start to have similar rates. A reasonable comparison appears between PMT-pairs

(a)   (b)
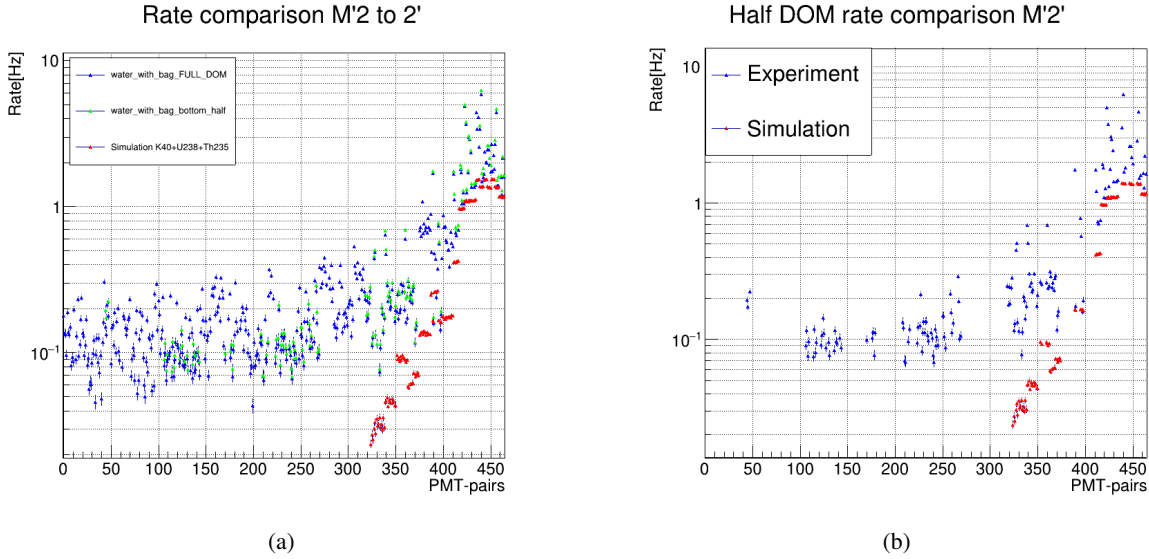
Figure 4.9: Rate comparison. (a) Rate produced by bottom hemisphere PMTs is compared to the rate produced by the whole experimental and simulated DOM. (b) Twelve PMTs from rows E and F of the DOM used for collecting data were muted as well as the equivalent PMTs for the DOM used in the simulation.

400 to 450. The rate in other PMT-pairs seems to be closer, but most of the pairs may be affected by a possible contamination of additional background sources still to be further verified.

As commented above, in an attempt to reduce a suspicious background of muons (likely the biggest contribution) that seemed to affect most of PMTs in the top hemisphere of the DOM, twelve PMTs were muted in total by re-writing the detector file (.detx) of the DOM, either for experimental and simulated data. The command used for this purpose was `JEditDetector -a <detector_file.detx> -P "<module iden-tifier> <PMT channel> set PMT_DISABLE" -o <new_detector_file.detx>`. Out of the 31 PMTs of the DOM, 19 PMTs remained active, this produced 171 PMT-pairs to correlate events instead of 465. At x-axis, the label of PMT-pairs count up to 465 instead of only up to 171 because PMTs still exist although data is discarded. Beside 465 independent PMT-pairs appear, only 171 are filled. This can be observed in Figure 4.9b, as there are pairs in blank. The total rate of correlated events drop almost in half to 99.78 Hz for the experimental data, and a little bit less abruptly for the simulation dropping to 48.93 Hz. Although rates get slightly closer by turning off PMTs, the rate caused by muons is removed significantly. In this point discrepancies are again corroborated, and allow the last conclusion of this work: *the experimental and simulated data is still non-matching, simulation accounts for constrained sources of light, in the other hand, a conventional black plastic bag for external sources isolation may not represent the best shielding. In this reasoning, a critical factor that may be affecting the results significantly leads to a suspicious background of atmospheric muons that might not be entirely rejected, but better*

accounted in the simulation for this work. In order to suppress the effect of the background produced by muons, a shielding for the experimental setup may be considered as a major issue.

Chapter 5

Conclusions

The aim of this thesis was to experimentally study the signature caused by radioisotopes, mainly from ^{40}K, contained in Vitrovex, the protective high pressure-resistant glass of DOMs. This study is relevant for KM3NeT collaboration since there are not enough experimental studies concerning ^{40}K contained in DOMs. This kind of study is very useful towards a better understanding of the optical background contribution recorded by the DOMs. The work performed in this thesis was conducted at Nikhef under controlled environment, prior the deployment of the DUs into the abyssal site of the Mediterranean Sea (KM3NeT operation site), providing useful insights about the *in-situ* performance of the DOMs.

Four experimental test bench configurations were built for the study of the radioactivity influence by ^{40}K in the KM3NeT DOMs. Results from experimental and simulated data show "reasonable discrepancies" suspected to be mainly caused by:

- A better description of the simulation to the most favoured experimental test bench configuration (Setup N4).

- Strongest contribution of an energetic external source different to Cherenkov events induced by ^{40}K decay in Vitrovex.

A conventional black plastic bag for isolation of external sources may not represent the best shielding. In this reasoning, a critical factor that may be affecting the results significantly leads to a suspicious optical background induced by down-going atmospheric muons that might not be entirely rejected, but better considered in the simulation for this work. In order to suppress the effect of a possible background component by down-going atmospheric muons, an improved shielding for the experimental setup may be considered as a major issue. The larger rate of events recorded by the PMTs looking upwards in the top hemisphere of the DOM may be associated to induced events by down-going atmospheric muons, a fact that must be further supported. If down-going atmospheric muons influence data, it was not strictly nor rigorously described in the simulations done for this work, indeed, linked to the fact experimental data interpretation is limited to the particular conditions used in the different setups.

Bibliography

[1] Silvia Adrián-Martínez, M Ageron, F Aharonian, S Aiello, A Albert, F Ameli, EG Anassontzis, M Anghinolfi, G Anton, S Anvar, et al. Deep sea tests of a prototype of the KM3NeT digital optical module. *The European Physical Journal C*, 74(9):3056, 2014.

[2] Luis A Anchordoqui. Ultra-high-energy cosmic rays. *Physics Reports*, 2019.

[3] Standard model. `https://www.physik.uzh.ch/en/researcharea/lhcb/outreach/StandardModel.htm`. Accessed: 2020-08-24.

[4] Ulrich F Katz and Ch Spiering. High-energy neutrino astrophysics: Status and perspectives. *Progress in Particle and Nuclear Physics*, 67(3):651–704, 2012.

[5] Bjrn Herold. *Simulation and Measurement of Optical Background in the Deep Sea Using a Multi-PMT Optical Module*. PhD thesis, Der Naturwissenschaftlichen Fakultat der Friedrich-Alexander-Universitat Erlangen-Nrnberg, 2017.

[6] Raj Gandhi, Chris Quigg, Mary Hall Reno, and Ina Sarcevic. Ultrahigh-energy neutrino interactions. *Astroparticle physics*, 5(2):81–110, 1996.

[7] Harold Yepes Ramírez. Characterization of the optical properties at the antares site using the optical beacon system. Influence on the detector performance. 2014.

[8] Claudio Giganti, Stéphane Lavignac, and Marco Zito. Neutrino oscillations: The rise of the pmns paradigm. *Progress in Particle and Nuclear Physics*, 98:1–54, 2018.

[9] Silvia Adrian-Martinez, M Ageron, F Aharonian, S Aiello, A Albert, F Ameli, E Anassontzis, M Andre, G Androulakis, M Anghinolfi, et al. Letter of intent for KM3NeT 2.0. *Journal of Physics G: Nuclear and Particle Physics*, 43(8):084001, 2016.

[10] Ivan Esteban, MC Gonzalez-Garcia, Michele Maltoni, Thomas Schwetz, and Albert Zhou. The fate of hints: updated global analysis of three-flavor neutrino oscillations. *arXiv preprint arXiv:2007.14792*, 2020.

[11] The sources of neutrinos. `https://lappweb.in2p3.fr/neutrinos/ansources.html`. Accessed: 2020-08-24.

[12] Abraham Loeb and Eli Waxman. The cumulative background of high energy neutrinos from starburst galaxies. *Journal of Cosmology and Astroparticle Physics*, 2006(05):003, 2006.

[13] J Abraham, P Abreu, M Aglietta, C Aguirre, D Allard, I Allekotte, J Allen, P Allison, J Alvarez-Muñiz, M Ambrosio, et al. Correlation of the highest-energy cosmic rays with the positions of nearby active galactic nuclei. *Astroparticle Physics*, 29(3):188–204, 2008.

[14] Michael F L'Annunziata. *Handbook of radioactivity analysis*. Academic press, 2012.

[15] SK Love. Natural radioactivity of water. *Industrial & Engineering Chemistry*, 43(7):1541–1544, 1951.

[16] MI Walker and KSB Rose. The radioactivity of the sea. *Nuclear Energy*, 29(4):267–278, 1990.

[17] Mahmoud A Radi Dar and Abeer A El-Saharty. Some radioactive-elements in the coastal sediments of the mediterranean sea. *Radiation protection dosimetry*, 153(3):361–368, 2013.

[18] MA Unland Elorrieta. Studies on dark rates induced by radioactive decays of the multi-pmt digital optical module for future icecube extensions. `https://www.uni-muenster.de/imperia/md/content/physik_kp/agkappes/abschlussarbeiten/masterarbeiten/1712-ma_munland.pdf`, 2017.

[19] PA Čerenkov. Visible radiation produced by electrons moving in a medium with velocities exceeding that of light. *Physical Review*, 52(4):378, 1937.

[20] Leif Rädel and Christopher Wiebusch. Calculation of the cherenkov light yield from low energetic secondary particles accompanying high-energy muons in ice and water with geant4 simulations. *Astroparticle Physics*, 38:53–67, 2012.

[21] Agata Trovato, Rosa Coniglione, Piera Sapienza, and Javier Barrios-Martí. Expectations for detection of neutrinos from point-like sources with km3net/arca. *PoS*, page 999, 2017.

[22] S Aiello, SE Akrame, F Ameli, EG Anassontzis, M Andre, G Androulakis, M Anghinolfi, G Anton, M Ardid, J Aublin, et al. Characterisation of the hamamatsu photomultipliers for the km3net neutrino telescope. *Journal of Instrumentation*, 13(05):P05035, 2018.

[23] Safety information for vitrovex glass material. `https://www.vitrovex.com/wp-content/uploads/2018/05/121018-Safety-Information-for-VITROVEX-glass-material.pdf`. Accessed: 2020-01-12.

[24] T Eder. *Simulationsstudien zum Untergrund durch radioaktive Zerfälle in einem optischen Modul mit mehreren Photomultipliern für IceCube-Gen2*. PhD thesis, B. Sc. Thesis, Westfälische Wilhelms-Universität Münster, Münster, 2016.

[25] Steven HD Haddock, Mark A Moline, and James F Case. Bioluminescence in the sea. 2009.

[26] Christian Tamburini, Miquel Canals, Xavier Durrieu de Madron, Loïc Houpert, Dominique Lefèvre, Séverine Martini, Fabrizio d'Ortenzio, Anne Robert, Pierre Testor, Juan Antonio Aguilar, et al. Deep-sea bioluminescence blooms after dense water formation at the ocean surface. *PloS one*, 8(7):e67523, 2013.

[27] Karlijn Kruiswijk et al. Bioluminescence at the km3net neutrino telescope. B.S. thesis, 2019.

[28] Dmitry Zaborov. The k-40 calibration method. *ANTARES internal notes, ANTARES-CALI/2011*, 1, 2011.

[29] White rabbit. `https://ohwr.org/project/white-rabbit/wikis/home`. Accessed: 2020-01-12.

[30] Jpp. `https://repository.asterics2020.eu/content/jpp`. Accessed: 2020-09-27.

[31] M Jamroży, M Gumiński, G Kasprowicz, R Romaniuk, and K Poźniak. White rabbit in space related application. In *Photonics Applications in Astronomy, Communications, Industry, and High-Energy Physics Experiments 2015*, volume 9662, page 96621B. International Society for Optics and Photonics, 2015.

[32] M. de Jong. Detector calibration. `https://common.pages.km3net.de/jpp/Detector_calibration. PDF`, 2019. Accessed: 2020-01-12.

[33] KM3NeT Data Analysis. `https://elog.km3net.de/Analysis/519`. Accessed: 2020-01-20.

Appendix A

Additional Material

PMT Id.	PMT Channel	x [cm]	y [cm]	z [cm]	ϕ [deg]	θ [deg]
F4	0	0	-17	15	56	-90
E5	1	-19	0	10	73	180
E4	2	-10	-17	10	73	-120
E3	3	10	-17	10	73	-60
F3	4	14	-8	15	56	-30
F5	5	-14	-8	15	56	-150
E2	6	19	0	10	73	0
F6	7	-14	8	15	56	150
F2	8	14	8	15	56	30
F1	9	0	17	15	56	90
E1	10	10	16	10	73	60
E6	11	-10	16	10	73	120
D1	12	0	19	-2	107	90
C1	13	8	14	-7	124	60
B1	14	0	10	-13	148	90
D2	15	16	10	-2	107	30
D6	16	-16	10	-2	107	150
C6	17	-8	14	-7	124	120
B6	18	-9	5	-13	148	150
B2	19	9	5	-13	148	30
C5	20	-17	0	-7	124	180
C2	21	17	0	-7	124	0
A1	22	0	0	-16	180	0
D3	23	16	-10	-2	107	-30
B4	24	0	-11	-13	148	-90
B3	25	9	-5	-13	148	-30
B5	26	-9	-5	-13	148	-150
D5	27	-16	-10	-2	107	-150
C4	28	-8	-14	-7	124	-120
C3	29	8	-14	-7	124	-60
D4	30	0	-19	-2	107	-90

Table A.1: Table showing the orientation of each PMT in the DOM used to take experimental data. (r, θ, ϕ)

Phase	Blocks	Primary deliverables
1	0.2	Proof of feasibility and first science results;
2	2	Measurement of the neutrino signal reported by IceCube; All flavour neutrino astronomy;
	1	Determination of the neutrino mass hierarchy;
3	6	Neutrino astronomy including Galactic sources;

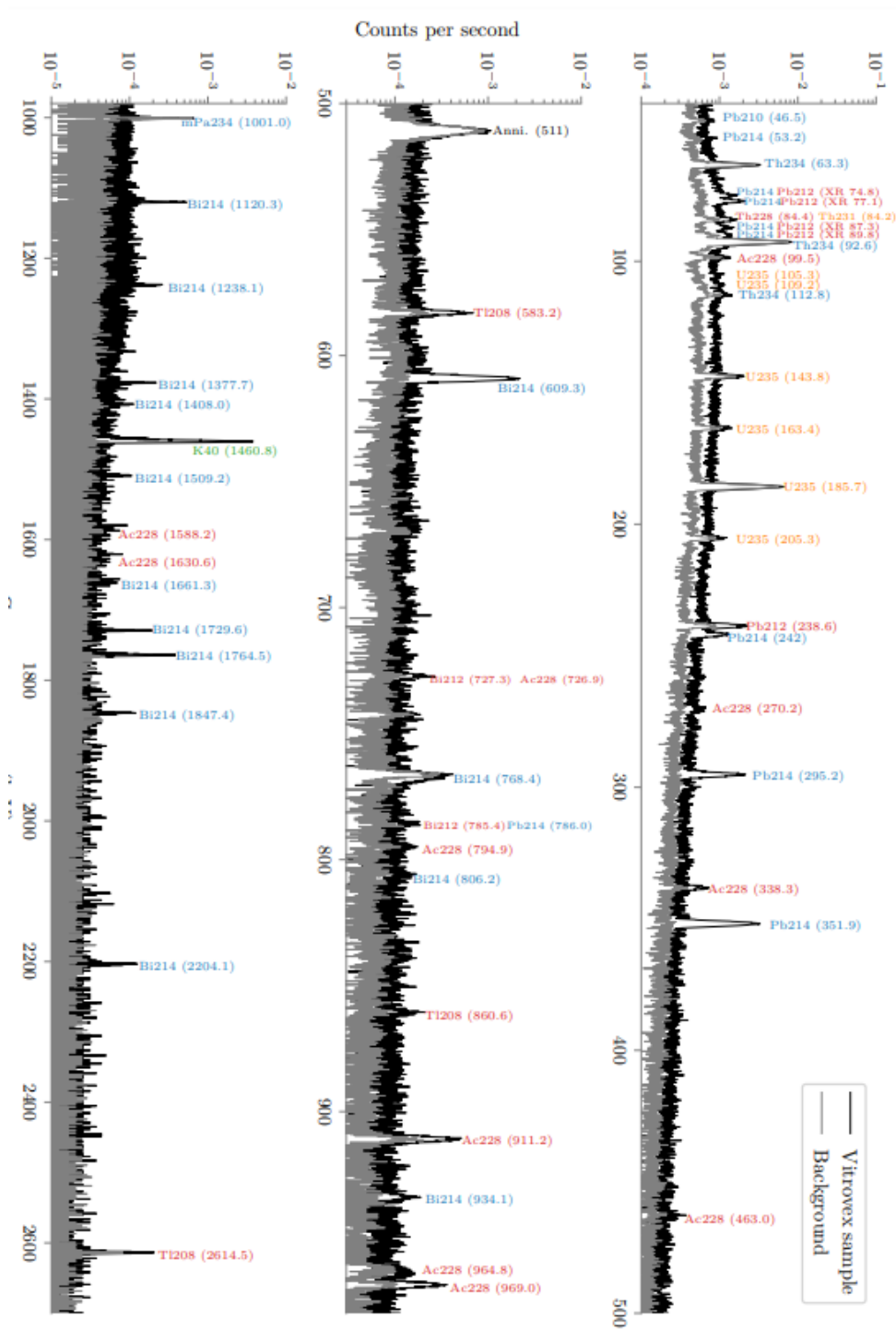Table A.2: Summary of the phased implementation of the KM3NeT research infrastructure

Figure A.1: Gamma spectrum for Vitrovex sample and background performed at the University of Alberta.[18]

Photo-cathode diameter	>72 mm
Nominal Voltage for gain $3 * 10^6$	$900/1300V$
Quantum Efficiency at 470 nm	$> 18\%$
Quantum Efficiency at 404 nm	$> 25\%$
Peak-to-Valley ratio	> 2.0
Transit Time Spread (FWHM)	< 5 ns
Dark count rate (0.3 spe threshold, at $20°$ C)	2000 cps max
Prepulses between -60 ns and -10 ns	1.5% max
Delayed pulses between 15 ns and 60 ns	5.5% max
Late afterpulses between 100 ns and 10 μs	15% max

Table A.3: Required characteristics for PMTs to be used in KM3NeT detectors. *spe* is for single photoelectrons, and *cps* is for counts per second.Table extracted from[22]